ÄSPÖLABORATORIET

INTERNATIONAL COOPERATION REPORT 94-05

Analysis of LPT2 using the Channel Network model

Björn Gylling[1], Luis Moreno[1], Ivars Neretnieks[1], Lars Birgersson[2]

1 Department of Chemical Engineering and Technology, Royal Institute of Technology, Stockholm, Sweden
2 Kemakta Konsult AB, Stockholm, Sweden

April 1994

Supported by SKB, Sweden

9505310279 950424
PDR WASTE
WM-11 PDR

SVENSK KÄRNBRÄNSLEHANTERING AB
SWEDISH NUCLEAR FUEL AND WASTE MANAGEMENT CO

BOX 5864 S-102 40 STOCKHOLM

TEL. +46-8-665 28 00 TELEX 13108 SKB TELEFAX +46-8-661 57 19

ISSN 1104-3210
ISRN SKB-ICR--94/5--SE

ANALYSIS OF LPT2 USING THE CHANNEL NETWORK MODEL

Björn Gylling[1], Luis Moreno[1], Ivars Neretnieks[1], Lars Birgersson[2]

1 Department of Chemical Engineering and Technoloy, Royal Institute of Technology, Stockholm, Sweden
2 Kemakta Konsult AB, Stockholm, Sweden

April 1994

Supported by SKB, Sweden

This document concerns a study which was conducted within an Äspö HRL joint project. The conclusions and viewpoints expressed are those of the author(s) and do not necessarily coincide with those of the client(s). The supporting organization has reviewed the document according to their documentation procedure.

102 8

ANALYSIS OF LPT2 USING THE CHANNEL NETWORK MODEL

Björn Gylling[1]
Luis Moreno[1]
Ivars Neretnieks[1]
Lars Birgersson[2]

April 1994

[1)] Department of Chemical Engineering and Technology
Royal Institute of Technology
S-100 44 Stockholm, Sweden

[2)]KEMAKTA KONSULT AB
Box 12655
S-112 93 Stockholm

KAT 93/16

ABSTRACT (English)

The Channel Network model was used to simulate the drawdown and the tracer tests which are parts of the Longterm Pressure and Tracer test, LPT2, carried out at the Äspö Hard Rock Laboratory. The input data used in the modelling was the data distributed by SKB to the Äspö Task Force groups. The influence of several boundary conditions and model parameters was tested. In the pressure test, for most cases, the simulated drawdowns were somewhat larger than those obtained in the experiment. The inflow to KAS06 was also used to compare the model results with the field test. The simulated inflow was larger, approximately by a factor of two. The simulation of the tracer tests resulted in a higher recovery of solutes in all cases. In the simulations the possible influence of the flow porosity and the diffusion in the rock matrix were also explored. The agreement between the simulation and the experiment was best for the test with injection in KAS12 section 2.

ABSTRACT (Swedish)

Kanalnätverksmodellen har använts för att simulera de pumptester och spårämnesförsök vilka är delar av det storskaliga experimentet "Longterm Pressure and Tracer test", LPT2 som har utförts vid Äspö Hard Rock Laboratory. De indata som har använts vid modelleringen har distribuerats av SKB till " Äspö Task Force"-grupperna. Inverkan av flera olika randvillkor och modellparametrar har undersökts. I det simulerade pumptestet blev "vattensänkningarna" generellt något större än de experimentellt uppnådda. Inflödet till KAS06 har också använts för att för att jämföra modellresultat med fältförsöket. Det simulerade inflödet var större med ungefär en faktor två. Simuleringen av spårämnesförsöket resulterade i ett större utbyte av spårämne i samtliga fall. I simuleringarna var också den möjliga inverkan av flödesporositeten och diffusionen i bergsmatrisen undersökta. Överenstämmelsen mellan simulering och experiment var bäst för spårämnesförsöket med injicering i KAS12 sektion 2.

TABLE OF CONTENTS

		Page
ABSTRACT		ii
TABLE OF CONTENTS		iii
SUMMARY		v
1	INTRODUCTION AND BACKGROUND	1
2	SITE CHARACTERIZATION	2
2.1	FRACTURE ZONES	2
2.2	BOREHOLES	4
3	THE CHANNEL NETWORK MODEL	6
3.1	GENERATION OF THE NETWORK	6
3.2	FLUID FLOW AT STEADY STATE	7
3.3	SOLUTE TRANSPORT CALCULATIONS	8
4	APPLICATION OF THE MODEL TO A SITE	10
4.1	THE MODEL SITE AREA	10
4.2	THE FRACTURE ZONES	10
4.3	THE BOREHOLES	11
4.4	BOUNDARY CONDITIONS	13
4.5	MODEL INPUT DATA	14
5	THE LPT2 EXPERIMENTS AT ÄSPÖ	17
5.1	THE PUMPING TEST	17
5.2	THE TRACER TEST	19
6	USE OF FIELD DATA TO OBTAIN MODEL PARAMETER VALUES	21
6.1	ESTIMATION OF THE CONDUCTIVITY DISTRIBUTION	21
6.2	ESTIMATION OF THE FLOW WETTED SURFACE	24
7	RESULTS	26
7.1	THE PUMPING TEST	26
7.1.1	Influence of the infiltration rate	27
7.1.2	Effect of higher conductivity on the upper model layer	29
7.1.3	Determined inflow to KAS06	32
7.1.4	Hydraulic head boundary conditions on the top surface	32

7.2 THE TRACER TESTS 35
7.2.1 The pathways for the solutes 37
7.2.2 Breakthrough curves 38
7.2.3 Some possible reasons for the scant recovery in tracer tests 44

8 **DISCUSSION AND CONCLUSIONS** 48

NOTATION 51
REFERENCES 52
APPENDIX 54

SUMMARY

The Channel Network Model is used to study the Longterm Pressure and Tracer test (LPT2) carried out in the Hard Rock Laboratory (HRL) at the island of Äspö. This test includes three major parts: several pumping tests, a tracer experiment and a tracer dilution experiment.

There are several identifiable fracture zones in the experimental site. The location of these fracture zones has preliminarily been determined by surface observations as well as geophysical and hydraulic methods. The fracture zones have been confirmed by investigations of the cores from the boreholes, by spinner and hydraulic head measurements and from observations during the tunnel excavation.

In the Channel Network Model, CNM, it is assumed that fluid flow and solute transport take place in a network of channels. Data for the model can be obtained from borehole transmissivity measurements and observations on fracture widths. One important aspect of the present model is that it is simple enough to be able to accommodate the transport of sorbing solutes and especially solutes that diffuse into the rock matrix and sorb in the interior of the matrix.

The dimensions of the model volume were chosen to be 1000·700·700 m in the south to north, east to west and downward direction, respectively. Our target volume starts at normal sea level and reaches a depth of 700 m. The model location was placed so that the most important boreholes in the LPT2 experiment, KAS01-02, KAS04-08 and KAS12, were included in the model.

The Longterm Pumping and Tracer test was performed with withdrawal of water in the open borehole KAS06. The maximum drawdown in borehole KAS06 was 51.77 m. When the pumping had created a steady state pressure head pattern the steady state drawdowns were measured in several boreholes. Most of them were divided into sections with packers, so that the drawdown could be obtained at a vast number of locations. In the drawdown simulation study, we have concentrated our interest to the boreholes KAS02, KAS04-KAS08.

When a steady hydraulic head gradient was developed, the tracer test was initiated. Injections were carried out in six borehole sections in KAS02, 05, 07, 08 and 12. The method of injection was either a decaying pulse injection or an intermittent decaying pulse injection. Four different tracers were used in the test; three radioactive isotopes and one fluorescent dye. Uranin injected in KAS12-2 and Rhenium-186 injected in KAS08-1 were

both clearly detected in KAS06. The other tracers were not observed in the withdrawal hole during the observation time.

Borehole data were used to obtain the standard deviation of the channel conductance distribution and the flow wetted surface. Data from the fracture zones and the rock mass were used to get the mean conductance for the respective locations. Owing to lack of data, some parameters had to be estimated based on previous experience from large field experiments.

Once the model was developed for the Äspö site using the data described above the steady state pumping tests were simulated. There were no calibrations or conditioning done in these simulations. When the particle following was carried out to simulate the tracer tests there was no attempt to perform any fitting or calibration in order to better match the experimental measurements at Äspö HRL.

We have simulated the steady state drawdown tests. Simulations of the transient pumping test were not performed. First, simulations were done with the CNM for the pressure tests. We have simulated the steady state drawdown tests. No simulations of the transient pumping test were performed. Several types of boundary conditions on the model ground level were tested, constant infiltration (10, 30 and 150 mm/year) and constant hydraulic head. A more conductive layer near the surface was also used in some simulations. When the experimentally determined hydraulic head was used in KAS06, a large inflow was obtained. A larger drawdown than in the field experiment was also, generally, obtained. Therefore, in a set of simulations the experimentally measured inflows to KAS06 were used, with a better agreement.

When tracer tests were simulated, a reasonably good agreement was obtained for the tracer injected in KAS12, section 2. In the tracer tests, the simulated concentrations were larger than the experimental ones. Considering that no adjustable parameters were used and that some entities such as the flow porosity and matrix diffusion properties were chosen based on previous experience from other sites, the deviations between experimental data and simulations are not surprising. In several cases, no tracer was detected in the experiment, whereas the output concentrations from the simulations were.

1 INTRODUCTION AND BACKGROUND

As a part of the SKB´s research programme in order to design a deep repository the building of an underground laboratory was initiated in the autumn of 1990. The facility Äspö Hard Rock Laboratory (HRL) is being constructed at this island near Simpevarp. Before the access tunnel of the HRL reached the island, various field experiments were performed in the area. One of these field experiments was the Longterm Pressure and Tracer test (LPT2). This test includes three major parts: several pumping tests, a tracer experiment and a tracer dilution experiment (Rhén et al., 1992).

A model for fluid and solute transport in fractured rock was developed (Moreno and Neretnieks, 1993). In the model, it is assumed that fluid flow and solute transport take place in a network of channels. The model is based on field observations in drifts and tunnels that show that there are strong channelling effects in fractured rock. These observations also show that flow channels are sparse and that the flow-rate distribution is very large among channels (Neretnieks et al., 1987). Fracture zones, tunnels, and boreholes may be included, in a simplified manner, in the model.

Model parameters may be estimated from field and laboratory measurements. Some of these measurements are performed in, or use boreholes e.g., hydraulic tests, core logs studies, spinner tests and tracer tests. Additional information may be obtained from studies of the flow-rate distribution of the various effluent points in tunnels and drifts and by measuring the width of the effluent channels. Tunnel observations may, however, be biased by stress changes and two-phase flow effects (Gylling et al., 1994). A method for obtaining the standard deviation in channel conductivity has been developed and used for data from Stripa, SFR and Kymmen. For these sites the channel length and width were also estimated (Moreno and Neretnieks, 1993). Data from borehole tests were also used to find the channel length.

The model is still at a development stage and the Äspö experiment gives a good opportunity to test the applicability of the Channel Network Model to a specific site. It has previously been applied to the study of water flow in the SCV Stripa experiment (Birgersson et al., 1992).

The aim of this paper is twofold:

- To apply the Channel Network Model to a specific site, Äspö, and
- to test the capability of the Channel Network Model to simulate the pressure and tracer tests performed at Äspö HRL.

2 SITE CHARACTERIZATION

The Äspö island seems to be divided in two parts, when it comes to the hydraulic situation, by a shear zone that has low conductivity in the direction perpendicular to the shear zone (Wikberg et al., 1991). A map of the area is shown in Figure 1. Generally, fracture zones that run from west to east seem to be different from those tending in a north to south direction. The former seem to be wider and contain more clay than the latter which are thinner. Occasionally they can be very conductive (Wikberg et al., 1991; Rhén, personal communication, 1993; and Bäckblom, 1993)

2.1 FRACTURE ZONES

The most important conductive structures on Äspö have been identified. The locations of these fracture zones have been preliminarily determined by surface observations, as well as geophysical and hydraulic methods. Fracture zones have been confirmed by investigation of the cores from the boreholes, by spinner and hydraulic head measurements and from observations during the tunnel excavation. The major fractures zones and their transmissivities are shown in Table 1. According to Wikberg et al. (1991), and more recent information from the tunnel excavation (SKB, 1993) and (Bäckblom, 1993), the major fracture zones may be described as below. Our main interest is focused on the zones within our simulation area. How the fracture zones are defined and included in the Channel Network Model is described in Chapter 4.

For the zone EW-1, the central part of that fracture zone has low permeability in the direction perpendicular to the striking direction of the fracture zone and coincides partly with the shear zone on the northern part of the island. EW-3 is a well defined and clay containing structure, but on the other hand EW-5 and EW-X seem to be very complex and undefined. EW-5 has not yet been found during the excavation but the pressure response shows that something must be there. The zone EW-X is judged as possible and not included in the simulation model. EW-7 is outside the boundaries of our model.

NE-1 on the southern part of the model is a very conductive zone and was confirmed during the excavation of the access ramp tunnel. NE-2 on the northern part of the island seems to have a twist, so that it has an inclination to the north on the western part of the zone and inclination to the south on the eastern part. NE-3 strikes towards north and has a moderate/low transmissivity. NE-4 is not included in our simulations.

NNW-1 and NNW-2 were not found by geological methods but hydraulic tests indicate that some zones are present there. Locally they have very high conductivities and are

located in the shear stress zone. Evidence of NNW-2 has been found in the tunnel. NNW–3 is not well defined, and thus judged as possible. NNW-4 was not found by geological methods but hydraulic responses might be explained by that zone. NNW-5 and NNW-6 are both determined to be possible and indicated by geophysical methods.

Table 1. The transmissivities for the fracture zones at Äspö (Wikberg et al., 1991).

Fracture zone	Transmissivity m^2/s
EW-1,W	$2.0 \cdot 10^{-5}$
EW-3,W	$5.0 \cdot 10^{-7}$
EW-5,W	$2.0 \cdot 10^{-5}$
NE-1,a	$2.0 \cdot 10^{-4}$
NE-1,b	$2.0 \cdot 10^{-4}$
NE-2,W	$4.0 \cdot 10^{-6}$
NE-3,W	$3.0 \cdot 10^{-5}$
NE-4,W	$3.5 \cdot 10^{-4}$
NNW-1,W	$1.5 \cdot 10^{-5}$
NNW-2,W	$4.0 \cdot 10^{-5}$
NNW-3,W	$2.0 \cdot 10^{-5}$
NNW-4,W	$4.0 \cdot 10^{-5}$
NNW-5,W	$5.0 \cdot 10^{-5}$
NNW-6,W	$5.0 \cdot 10^{-5}$
EW-7	$1.4 \cdot 10^{-4}$
NW-1	$7.0 \cdot 10^{-6}$

2.2 BOREHOLES

In order to study the structure of the Äspö site area, before the construction of the access tunnel to the HRL, several boreholes were drilled. Some of these boreholes are used in the pressure and tracer tests. Knowledge of the location where these boreholes intersect the fracture zones is of vital importance in the simulations. It is expected that most of the flow and tracer transport occur through the fracture zones.

In the pressure and tracer tests called LPT2, the borehole KAS06 had a very important role. It is used as pumping hole in these tests. One kind of useful information which may be used in the simulations of the LPT2 is the location and the size of the water inflow to the pumping hole. Nine of the largest inflows and their locations are shown in Table 2 below.

Table 2. Locations of inflow to KAS06 from spinner and packer tests (Forsmark, 1992).

Conductive zone	Length along the hole from the top m	Percentage of total inflow
1	65	15.0
2	217	20.9
3	312	5.6
4	353	15.3
5	364	25.8
6	399	8.4
7	448	4.2
8	558	3.5
9	596	1.3
Total		100.0

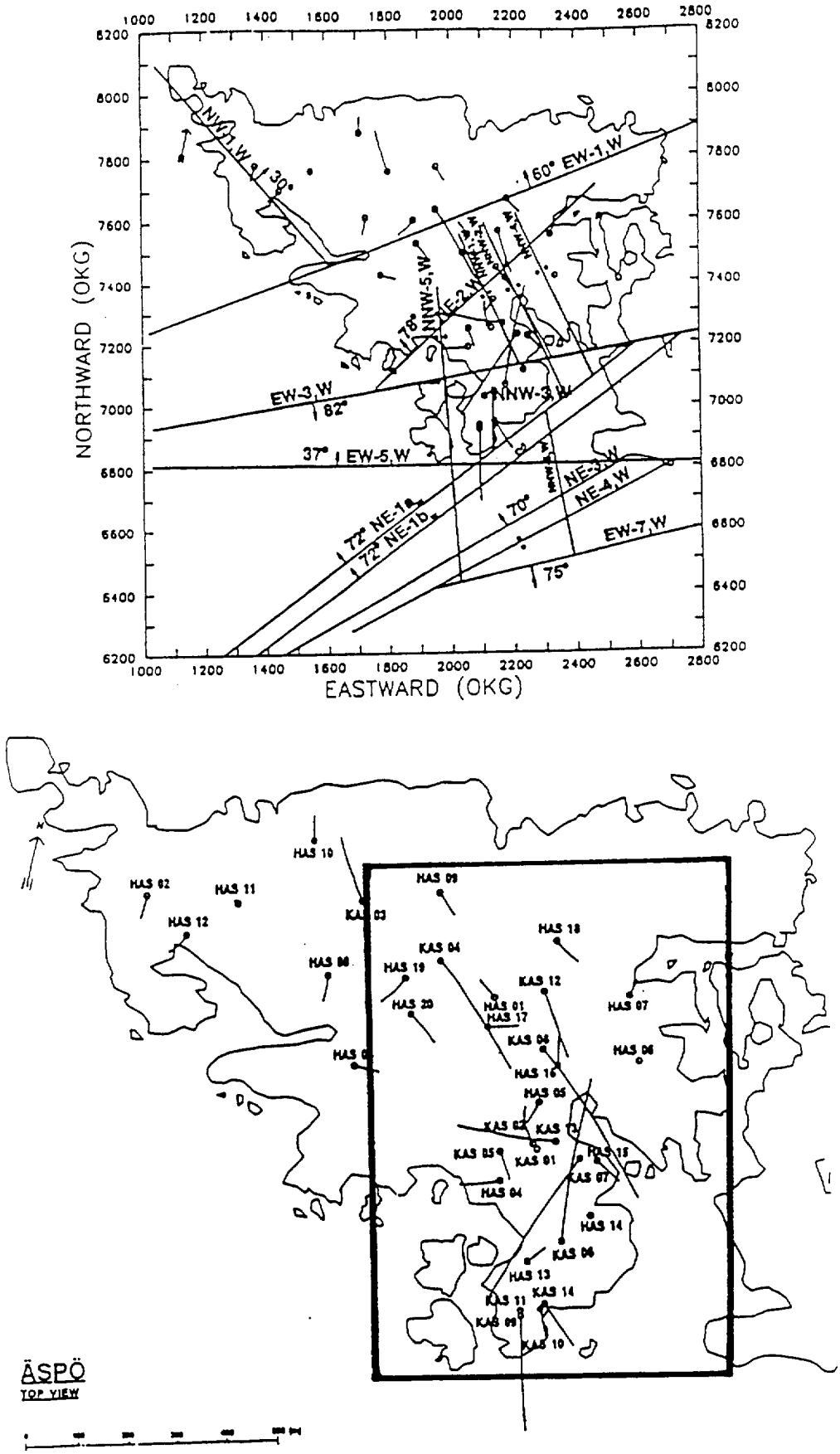

Figure 1. Major fracture zones and boreholes at Äspö. The modelled zone is marked with the rectangle. The maps are from Rhén et al., (1992).

3 THE CHANNEL NETWORK MODEL

In the model concept it is assumed that fluid flow and solute transport take place in a network of channels. With this simplification, a simple model is developed that does not need very detailed information. Data can be obtained from borehole transmissivity measurements and observations on fracture widths. One of the important aspects of the present model is that it is simple enough to be able to accommodate the transport of sorbing solutes and especially solutes that diffuse into the rock matrix and sorb in the interior of the matrix.

It is assumed that the flow paths make up a channel network in the rock. Every channel member can connect to any number of other channel members, but we choose an upper limit of six members intersecting at a point. Some of these channel members may have a conductivity that is so low that no connection is made. The use of six channel members is partly based on the observation that both fracture intersection and channels in the fracture planes play an important role in conducting flow. This is illustrated in Figure 2.

For visualization purposes, the network is depicted as a rectangular grid. The hydraulic properties of the members can be generated by including the effects of channel members of different lengths, different hydraulic conductivities and other properties of interest. The channel density may be varied in different regions, e.g., along the fracture zones. These properties allow us to define, in a straightforward way, fracture zones.

3.1 GENERATION OF THE NETWORK

Each member of the network is assigned a hydraulic conductance. This is the only entity needed to calculate the flow, if the pressure field is known. The conductance is defined as the ratio between the flow in a channel and the pressure difference between its ends. If the residence time for non-interacting solutes is to be calculated, then the volume of the channel members is needed as well. If sorption onto the fracture surface or diffusion into the matrix will be included in the model, the surface area of the flow wetted surface must also be included. Then some properties of the rock are needed, such as rock matrix porosity, diffusivity, and sorption capacity for sorbing species (Neretnieks, 1980).

Here, the conductances of the channel members are assumed to be log-normally distributed, with mean μ_0 and standard deviation σ_C. It is also assumed that the conductances are not correlated in space. Different values are used for the mean

conductance μ_0, depending whether on the channel member is located in a fracture zone or in good rock. Channels located in a fracture zone have larger hydraulic conductivity than if they are in the rock mass. For tracer transport calculations, a relationship between the channel volume and conductance is assumed, owing to lack of data. We have previously tested different relationships.

Figure 2 shows a schematic view of the mesh used in this report. An outline of the approach used to calculate the fluid flow and solute transport through the network of members is presented below. The method is described in more detail in Moreno and Neretnieks (1993).

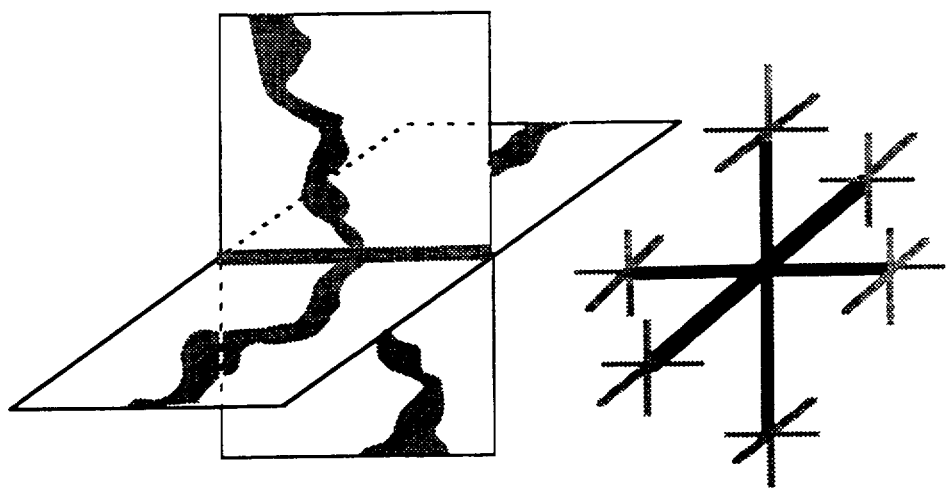

Figure 2. A schematic view of the mesh used, each node is connected to up to six other nodes.

3.2 FLUID FLOW AT STEADY STATE

For laminar conditions, the flow through a channel is proportional to the pressure gradient:

$$Q_{ij} = C_{ij}(P_j - P_i) \qquad (1)$$

where Cij is the conductance of the channel connecting the nodes "i" and "j". The pressure field is calculated by writing the mass balance at each intersection point:

$$\sum_j Q_{ij} = 0 \quad \text{for all i} \tag{2}$$

The solution of this system of equations yields the pressure at each node. For the numeric solution of the system of equations a code developed by Moridis (personal communication, 1992) was used. Flow between adjacent nodes is then calculated using Equation (1).

3.3 SOLUTE TRANSPORT CALCULATIONS

The solute transport is simulated by using a particle-following technique (Robinson, 1984; Moreno et al., 1988). Many particles are introduced, one at a time, into the known flow field at one or more locations. Particles arriving at an intersection are distributed in the outlet channel members with a probability proportional to their flow rates. This is equivalent to assuming total mixing at the intersections. Each individual particle is followed through the network. The residence time for non-sorbing tracers in a given channel is determined by the flow through the channel member and by its volume. The residence time of an individual particle along the whole path is determined as the sum of residence times in every channel member that the particle has traversed. The residence time distribution is then obtained from the residence times of a multitude of individual particle runs. Hydrodynamic dispersion in the channels is considered to be negligible.

From the RTD, the mean residence time and variance may be calculated. They may be used to determine the Peclet number, which is a dimensionless measure of the dispersivity (Levenspiel, 1972):

$$\frac{2}{Pe} = \frac{\sigma_t^2}{t_w^2} \tag{3}$$

When dispersion in the channel and/or diffusion into the rock matrix are considered, different particles in the same channel member will have different residence times. Here, residence times for the particles may be described by the RTD of the particles, expressed as a probability density function, pdf. It may be thought of as the outlet concentration for a pulse injection. If this curve is integrated over all the possible residence times, the cumulative distribution of the residence times is obtained.

For a flat channel from which the diffusion is perpendicular to the channel surface, a simple analytical solution is available for the RTD. The cumulative curve, F, for the residence times is obtained as:

$$F = \mathrm{erfc}\left(\frac{(K_d\, D_e\, \rho_p)^{0.5}\, L\, W}{(t - t_w)^{0.5}\, Q} \right) \qquad (4)$$

for values greater than the water-plug-flow residence time (Carslaw and Jaeger, 1959). Otherwise, the value is zero. Equation (4) considers only advection in the channel and diffusion into the rock matrix. Longitudinal dispersion is neglected.

For particle following, we follow the technique used by Yamashita and Kimura (1990). The travel time for each particle in a channel member is determined by choosing a uniform random number in the interval [0,1]. The travel time for the particle, t, is then calculated by solving for t in Equation (5):

$$[R]_0^1 = \mathrm{erfc}\left(\frac{(K_d\, D_e\, \rho_p)^{0.5}\, L\, W}{(t - t_w)^{0.5}\, Q} \right) \qquad (5)$$

4 APPLICATION OF THE MODEL TO A SITE

4.1 THE MODEL SITE AREA

The Longterm Pressure and Tracer tests, LPT2, were performed at the island of Äspö, in the area where the Äspö Hard Rock Laboratory is under construction. A map of the area indicating the modelled zone is shown in Figure 1. The dimensions of the model volume were chosen to be 1000·700·700 m in the south to north, east to west and downward direction, respectively. Our target volume starts at normal sea level and reaches a depth of 700 m. The model was placed so that the most important boreholes in the LPT2 experiment, KAS01-02, KAS04-08 and KAS12, were included in the model. The boreholes mentioned are shown in Figure 3. The borehole KAS03 was omitted because there seems to be a different flow situation in the northern part of the Äspö island compared to the southern part, and the connection cross-over the shear zone that divides the island seems to be weak. The northern borderline of our model is roughly located at this dividing structure. In order to avoid the effects from the boundary conditions some distance is added to the vertical sides so that a suitable distance is kept between the boreholes and where we set our model boundary conditions.

4.2 THE FRACTURE ZONES

The dominating water flow paths are determined by the major fracture zones. These fracture zones are responsible for most of the water flow. The modelled fracture zones are shown in Figure 15. Thirteen of the largest fracture zones that have been found are included in the simulation model. The properties of the different zones are described in short in Chapter 2, Site Characterization. In the model, we have assumed that the fracture zones may be described by two parallel planes delimiting the zone with high permeability. Channels included between these two limiting planes have higher conductances than channels in the "good" rock. Conductances are taken from a distribution with a mean value that matches the experimentally estimated transmissivity of the fracture zone. The fracture zone widths used for all fracture zones are about 2.5 channel lengths which is equal to 50 m in this case. In order to support a good connection along the fractures zone it would not be possible have a smaller number of channels. The fracture zone widths can, however, be decreased by using a shorter channel lengths. The actual width of the zone has little influence on the result in comparison to the conductances, apertures and widths of the channels.

One of the main parameters in the Channel Network Model is the distribution of channel conductances, from which we need the first and the second moments i.e, the mean value, μ_O, and the standard deviation of the channel conductances, σ_C. A log-normal distribution for channel conductances is assumed in these calculations. The mean log conductance for channels within the fracture zones is calculated from the transmissivity data, shown in Table 1. The value of σ_C for channels describing the fracture zones in the site is estimated with help of data from the borehole measurements, as described in Chapter 6.

The mean conductance for channels within the rock mass is calculated from the rock mass conductivity obtained by Wikberg et al., (1991). The value of standard deviation in channel conductances used for the good rock mass is taken to be similar to that used for the fracture zones. The choice of this value is not critical because the mean conductivity of the rock mass is considerably smaller if compared with that of the fracture zones, so these channels do not play an important role in the flow simulations. A small value of the standard deviation for conductance of channels in good rock is also tested; this would be advantageous from a numerical point of view.

4.3 THE BOREHOLES

The seven boreholes included in the model are KAS02, KAS04-08 and KAS12. The withdrawal of water was carried out in KAS06 and the rest of the holes are used for measurement of the hydraulic head response. Some are used for tracer tests. Most of the holes are equipped with packers so that the hydraulic head can be read at various locations along the borehole. The magnitude of the hydraulic head value in a given packer interval is determined by the largest conductive zones that the borehole intersects within the packer section. In most of the cases only one high conductive zone is found in each interval. The location, as the distance along the borehole, of these high conductive zones in the boreholes is shown in Table 3. This type of detailed information was not found for KAS12.

When more than one highly conductive zone is found, in a measurement section between two packers, they will be connected by the borehole which will act like a highly conducting channel. The hydraulic head readings for such sections will be influenced by contributions from each conductive point. This is the reason why there sometimes are two distances for a specific packer section in Table 3. In some packers more than two large conductivities were found, but in the simulations only the two largest values have been considered. An exception to this is the value for the withdrawal hole, which had nine conductive inflow points. The locations for these are shown in Table 2.

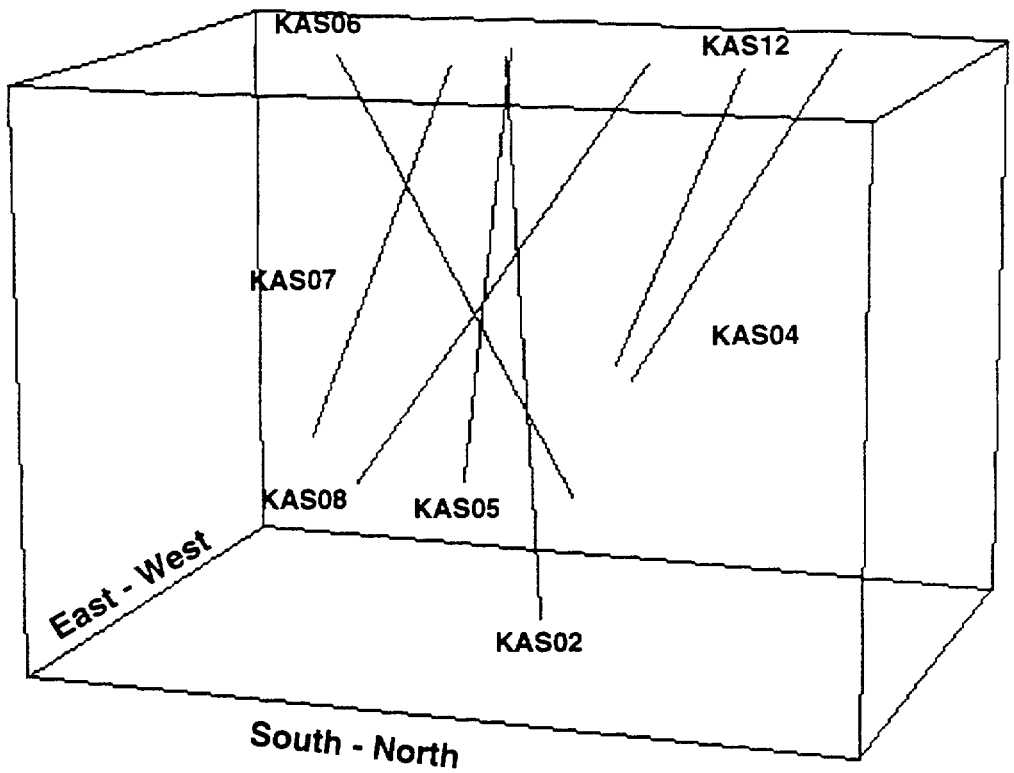

Figure 3. Schematic picture of the model volume and the most important boreholes used in the simulations.

Table 3. Distance along the boreholes, in meters, from the top of the hole to the most conductive zones within different packers for the boreholes KAS 02, KAS04 - 08.

Borehole	Packer 1	2	3	4	5	6
KAS02			456	315	194	
KAS04	427	338 380	296	254	191	151 178
KAS05	442 466	437	328 364	229 304	169	
KAS07	562	431		241	127 173	
KAS08			148 187	463	564	

4.4 BOUNDARY CONDITIONS

We have used and tested various types of boundary conditions in the calculations. The type of condition used depends on which side of the model it is located at. On the top of the model block we have mainly used a specified inflow condition due to infiltration caused by precipitation. The assumed amount of water flowing in is based on the precipitation, the evaporation and the run-off. In some simulations we have also tested a constant hydraulic head boundary condition on the upper side. On the vertical surfaces around the block a constant hydraulic head condition is used, and at the bottom of the model a non-flow condition is used. Two approaches were tested as boundary condition in the pumping hole. In most of the simulation sets the maximum drawdown in KAS06 was used. In another set of simulations we have set a predetermined inflow condition at the locations which have been found to be water bearing in the experimental study. In this case, the simulated inflow values are set equal to the corresponding experimental ones.

4.5 MODEL INPUT DATA

As discussed above, an important parameter of the model is the distribution of channel conductances. The mean value, μ_0, may be estimated from conductivity and transmissivity data. There will be one value of μ_0 applicable for the channels within the rock mass and a particular μ_0 for each fracture zone. The standard deviation may be estimated by using observations from drifts or tunnels or from borehole hydraulic measurements. These two approaches are described in detail in earlier papers (Moreno and Neretnieks, 1993; Gylling et al., 1994). These methods are briefly described below.

In general, to estimate the standard deviation in conductances results from simulations are matched with experimental values. Simulations are made for several values of standard deviation and they are compared with the observations in tunnels or hydraulic borehole measurements. As a base for the comparison, the cumulative flow into the drift as a function of the flow rate may be used. The cumulative number of channels as a function of the flow rate may be used as well. In both cases we start the comparison from the largest flow rates, since the small flow rates are difficult to measure. Below, we present a procedure that allows us to estimate the standard deviation of channel conductance and the channel length.

The flow rates out from the simulated cubic grid cover a very wide interval, if a large value of σ_C is used. On the other hand, the flow into the drift measured in the field often show variations of only a few orders of magnitude in flow rates. This aspect is schematically presented in Figure 4. The histogram shows the number of channels with flow rates in a given interval, if even the channels with a very small flow rate could be monitored. Data for only six to eight bins may be obtained from field observations. They are the gray bars in the figure. The white bars represent the unknown data. The whole histogram could also represent the results of a simulation.

The σ_C estimation procedure is as follows: The inflow measurements to the drift are compared with the simulated results for different σ_C:s. With the available data (the gray bars) the standard deviation σ_C may be estimated by matching simulated and observed data. Then, when the value of σ_C is known, the number of channels in the observable flow-rate interval for the field data is compared with that of the model for the same interval. The total number of channels in the field (observable and non-observable channels, or gray and white bars in the histogram) is obtained by comparing the field data with the results from simulations.

$$\frac{\text{Total number of channels in rock}}{\text{Total number of channels in simulations}} = \frac{\text{Number of channels observed in rock above a chosen flowrate}}{\text{Number of channels in the simulations spanning the same flowrate range}} \qquad (7)$$

The same procedure may be used for packer test data from boreholes if these are analysed for the number of intersections and the size of the inflow, provided that the channel widths and the borehole diameter are known.

We attempted to use a non-linear least square fitting technique to match the data and to obtain μ_O, σ_C and the number of non-observable channels. This was not always successful, therefore a "manual" matching procedure was developed.

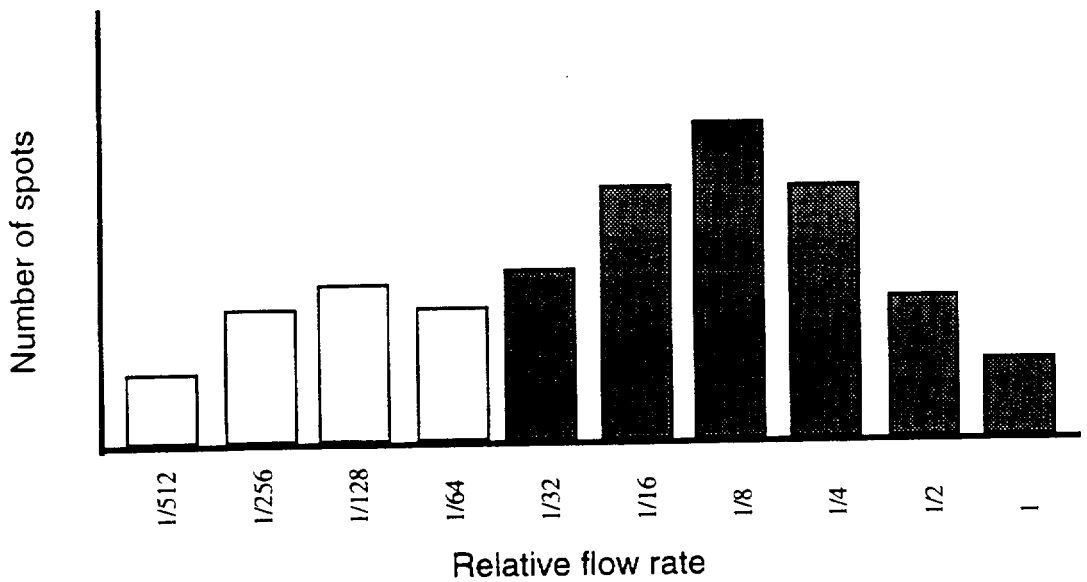

Figure 4. Histogram showing the number of channels with a flow rate in a given interval. The gray bars represent hypothetical data from field observations. The white bars represent channels with a flow rate below the detection limit. Note that the flow rate axis is logarithmic.

This matching procedure using tunnel and drift data was, for example, used to calibrate the Channel Network Model to SFR and Stripa data. The cumulative number of channels with flow larger than a given flow rate is calculated for the experimental data and simulations. The ratios between the number of cumulative channels in the observations and in the model are obtained as a function of the flow rate. This is done for several different values of σ_C. When the ratio between observation and simulation is approximately the same, over the total flow interval the model, σ_C is found. Figure 5 shows approximately the same value for this ratio over the whole conductivity range for a σ_C of 1.6.

By observing the number of leaking points on the tunnel walls in SFR-site, an estimation of the channel length was done. From the number of channels, and the total surface area of the tunnel sides and ceiling, the channel density was determined as one channel per 2.7 m^2. The channel length was then estimated to be the square root of the channel density. In this case the channel length was determined to 1.6 m.

In the analysis of the Äspö LPT2 experiment the estimation of the σ_C for the model was done by using measurements of hydraulic conductivity in the boreholes. Transmissivity data for fracture zones and hydraulic conductivity for the rock mass were used to get the mean channel conductivity at the respective location. σ_C for the model rock mass channels was assumed to be equal to that in the fracture zone owing to lack of data. Inflow data from the access tunnel is not available or not detailed enough for our purposes. The rock around a drift or a tunnel may be disturbed and the observation may have been influenced by several phenomena related to skin, air intrusion, rock stresses closing or opening channels etc. It might therefore be more appropriate to use data from boreholes.

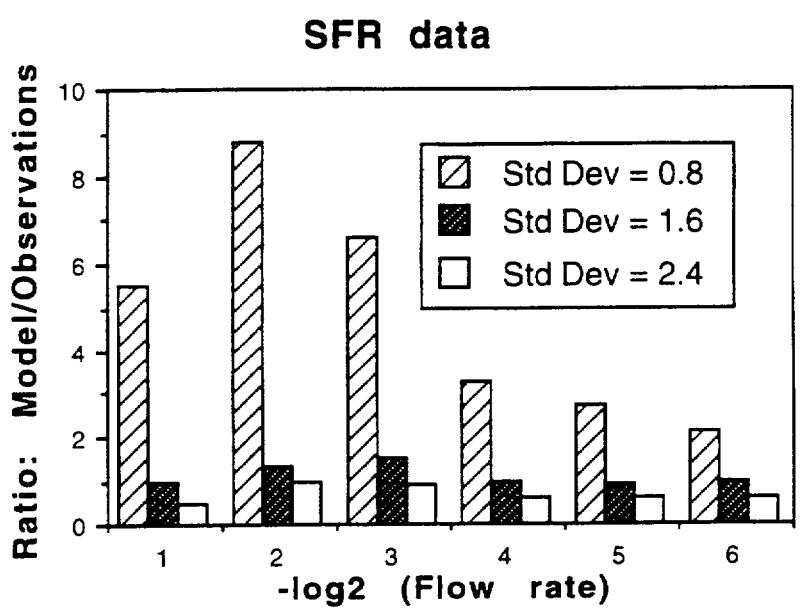

Figure 5. Ratio of model to observed number of channels in SFR for different standard deviations, σ_C.

5 THE LPT2 EXPERIMENTS AT ÄSPÖ

Within the frame of LPT2, three tests were carried out at Äspö, namely several pumping tests, a dilution test and a tracer test. In this report we will only consider the pumping and the tracer test.

5.1 THE PUMPING TEST

The Longterm Pumping and Tracer test was performed with withdrawal of water in the open borehole KAS06, which is 602 m long and dips 60° towards north. The duration of the pumping test was three months, between September and December 1990. The maximum drawdown in borehole KAS06 was 51.77 m. When the pumping had created a steady state pressure head pattern the steady state drawdowns were measured in several boreholes. Most of them were divided into sections with packers, so that the drawdown could be obtained at a vast number of locations. The flow rate was changed twice, in order to obtain an optimal drawdown in the withdrawal hole for the tracer tests, (Forsmark, 1992). This is shown in Table 4.

In this simulation study, we have concentrated our interest on the cored boreholes KAS02, KAS04-KAS08 for the drawdown tests. The drawdowns in the boreholes were monitored and the connections were classified as good, intermediate, poor and no response (Rhén et al., 1992). In boreholes KAS02, KAS05, KAS07, KAS08 and KAS12 some sections with good connection were found. In KAS01, KAS09 and KAS11 the responses were intermediate, and in KAS03 and KAS10 the responses were poor. The drawdown at different locations is shown in Table 5, and can also be seen in e.g., Figures 9 to 13, together with the result from one of the simulations.

Table 4. Average pumping flow rate during the LPT2.

Period (min)	Flow rate (m^3/s)	Flow rate (m^3/a)
0 - 4 320	$2.01 \cdot 10^{-3}$	63 387.4
4 320 - 10 439	$2.52 \cdot 10^{-3}$	79 470.7
10 439 - 132 595	$2.25 \cdot 10^{-3}$	70 956.0

Table 5. Drawdown in the boreholes KAS02, KAS04-08 for the sections studied in the simulations. Experimental data taken from Rhén et al., (1992).

Borehole section	Distance from KAS06 (m)	Drawdown (m)
KAS02 -5	114	5.79
-4	131	6.30
-3	338	5.40
-2	584	2.41
-1	645	2.30
KAS04 -6	479	0
-5	397	3.27
-4	362	3.11
-3	327	3.42
-2	301	3.58
-1	277	3.33
KAS05 -5	223	5.58
-4	133	4.97
-3	156	5.45
-2	195	3.30
-1	264	3.06
KAS06 -1	0	51.77
KAS07 -5	137	16.53
-4	112	5.61
-3	165	1.69
-2	253	1.88?*
-1	343	2.54
KAS08 -3	200	6.58
-2	97	4.70
-1	226	3.74

* Uncertain data.

5.2 THE TRACER TEST

About two weeks after that the pumping test started, a steady hydraulic head gradient was developed so that the tracer test could be initiated. The injections were carried out in six borehole sections in KAS02, 05, 07, 08 and 12. Table 6 shows the locations of the injection,. the type of injection used and the injected tracer. The method of injection was either a decaying pulse injection or an intermittent decaying pulse injection, called pulse and intermittent, respectively, in the table. Four different non-sorbing tracers were used in the test; three radioactive isotopes and one fluorescent dye. The tracers used were In-114, I–131, Re-186 and Uranin. In-114 is a metal complex with EDTA, and I-131 and Re-186 exist as negative ions, I^- and ReO_4^-, respectively. For the experimental conditions and observations we refer to Rhén et al., (1992).

The breakthrough curves for the solutes arriving at the withdrawal borehole are determined for the total discharge and for the different levels. The concentration of the tracer in the total discharge is very low because the tracer is diluted in the total amount of water flowing into KAS06. Uranin injected in KAS12-2 (section DB, 279-329 m) and Rhenium-186 injected in KAS08-1 (section M1, 503–601 m) were clearly detected in KAS06. Uranin injected in KAS05-3 (section E3, 320-380 m) is not clearly detected in the withdrawal borehole. The breakthrough curves for Uranin and Rhenium, in KAS06 for the total discharge, are shown in Figures 6 and 7. The tracer recovery was 38 and 2.1 % for the tracer injected in KAS12-2 and KAS08-1 respectively.

Table 6. The locations for injections, methods and tracers used for the tracer tests, the tests that resulted in clear detection in bold style.

Borehole	Packer interval	Method	Tracer
KAS02	4	Pulse	Indium-114
KAS05	3	Pulse	Uranin
KAS07	4	Intermittent	Iodine-131
KAS08	**1**	**Intermittent**	**Rhenium-186**
KAS08	3	Pulse	Rhenium-186
KAS12	**2**	**Intermittent**	**Uranin**

ABSTRACT

A stable isotope ($\delta^{13}C$, $\delta^{18}O$, $\delta^{34}S$) study combined with radiogenic ($\delta^{87}Sr$) isotopes on ground water and calcite fracture fillings at Äspö, southeastern Sweden, suggest that several end-members have been involved in the ground water formation. None of the isotope signatures of the present ground water resemble those of modern Baltic sea water although the possibility of mixing between Baltic sea water and shallow ground waters cannot be excluded. The large range in $\delta^{13}C$ values in the carbonate system is indicative of multiple sources for the carbon, including atmospheric, organic and methane derived carbon. The $\delta^{18}O$ signatures in the water as well as in calcite fracture fillings suggest mixing of meteoric and marine waters, but most of the calcites are precipitated from waters with $\delta^{18}O$ values similar to those of present-day ground water. The $\delta^{34}S$ values of the dissolved sulphate indicate a multiple sulphur source, including marine, non-marine and bacterially reduced sulphur. The 1.8-Ga host rock at Äspö is characterized by low Rb/Sr ratios, and a calculated mean $\delta^{87}Sr$ demonstrates a lack of isotopic equilibrium between the ground water and the host granite at the bulk rock scale although preferential mineral dissolution is possible. Calcite fracture fillings add further complexity to the Sr-isotope budget. The most significant result of this study is that several waters have been involved in the formation of the calcite fissure fillings at Äspö. This indicates a complex paleohydrology which must be better understood if credible predictions of future hydrology are to be made. Finally, this study demonstrates that a comprehensive isotopic approach to ground water studies utilizing a combination of stable and radiogenic isotopes can yield critical and relevant data for developing an understanding of the origin and evolution of the ground water at Äspö in particular and in the circum-Baltic region in general.

CONTENTS

		Page
	SUMMARY	i
1.	INTRODUCTION	1
2.	GEOLOGICAL SETTING, FRACTURES AND FRACTURE FILLINGS	3
3.	HYDROCHEMISTRY	3
4.	METHODS	4
4.1.	Sample Collections	4
4.2.	Analytical Work	4
4.2.1.	^{13}C-, $d^{18}O$-analyses	4
4.2.2.	$d^{34}S$-analyses	4
4.2.3.	$d^{34}S$-analyses	5
5.	RESULTS	5
6.	DISCUSSION	5
6.1.	*FRACTURE MINERALS*	5
6.1.1.	*^{13}C-isotopes in calcites*	7
6.1.2.	*$d^{18}O$-isotopes in calcites*	7
6.1.3.	*^{87}Sr-isotopes*	7
6.1.4.	*Laser analyses*	8
6.2.	*GROUND WATER*	10
6.2.1.	*$d^{18}O$- and D-isotopes*	16
6.2.2.	*^{34}S-isotopes in dissolved sulphates*	17
6.2.3.	*^{87}Sr-isotopes*	17
6.3.	*ISOTOPIC EVOLUTION OF THE PALEOBALTIC*	18
7.	CONCLUSIONS	20
8.	ACKNOWLEDGEMENTS	21
9.	REFERENCES	22

CONTENTS Page

	SUMMARY	i
1.	INTRODUCTION	1
2.	GEOLOGICAL SETTING, FRACTURES AND FRACTURE FILLINGS	3
3.	HYDROCHEMISTRY	3
4.	METHODS	4
4.1.	Sample Collections	4
4.2.	Analytical Work	4
4.2.1.	*^{13}C-, d^{18}0-analyses*	4
4.2.2.	*d^{14}S-analyses*	5
4.2.3.	*d^{34}S-analyses*	5
5.	RESULTS	5
6.	DISCUSSION	7
6.1.	*FRACTURE MINERALS*	7
6.1.1.	*^{13}C-isotopes in calcites*	7
6.1.2.	*d^{18}0-isotopes in calcites*	8
6.1.3.	*^{87}Sr-isotopes*	10
6.1.4.	*Laser analyses*	16
6.2.	*GROUND WATER*	17
6.2.1.	*d^{18}O- and D-isotopes*	17
6.2.2.	*^{34}S-isotopes in dissolved sulphates*	18
6.2.3.	*^{87}Sr-isotopes*	20
6.3.	*ISOTOPIC EVOLUTION OF THE PALEOBALTIC*	21
7.	CONCLUSIONS	22
8.	ACKNOWLEDGEMENTS	23
9.	REFERENCES	23

SUMMARY

This progress report summarizes the results of a comprehensive stable (O, H, S, and C) and radiogenic (Sr) isotopic investigation of ground water and calcite fracture fillings at the SKB´s Äspö Hard Rock Laboratory. The integration of these isotopic techniques, along with water quality data, provides a powerful approach for understanding the origin and evolution of the ground water and the hydrogenic minerals deposited in fractures. The fracture fillings mark the pathways of past fluid movement so an understanding of their genesis is particularly important for understanding the paleohydrogeology of the area. The utility in applying the multiple-isotope to ground water and fracture minerals derives from the fact that the different systems represent different processes. Oxygen and hydrogen isotopes in ground water at low temperatures are considered to be conservative with little modification by water-rock interaction. Hence, they reflect the values of water or waters recharged into the system. Dissolved carbon is derived largely through atmospheric input or by solution of CO_2 in the soil zone during infiltration. Among the stable isotopes, sulphur may exhibit the most complex behavior because of its multiple valence states, its amenability to bacterial fractionation. Strontium is a dissolved species geochemically analogous to calcium. The variability of strontium in ground water results solely from dissolution of or exchange with minerals during infiltration and along the flow paths. In addition to sourcing the ground water, O, C, and Sr provide important constraints on identifying the water from which the hydrogenic deposits precipitated. Sr isotopes do not fractionation with phases changes, and the fractionation of O isotopes can be readily calculated. If multiple but isotopically distinct waters are present, all of these systems are helpful in identifying mixing.

Ground water and calcite fracture fillings at Äspö. None of the isotope signatures resemble those of modern Baltic sea water although the possibility of mixing between Baltic sea water and shallow ground waters cannot be excluded. D values ranges between -112 to -55 o/oo and $\delta^{18}O$ values range between -7 and -15 o/oo. The $\delta^{13}C$ of the bicarbonate range between -16 and -6 o/oo , and decrease systematically with depth suggesting mixing of organic and inorganic carbon. The ^{18}O of the bicarbonate is uniform (+18 and +22 o/oo) and in equilibrium with the most of the ground water. $\delta^{34}S$ values of the dissolved sulphate varies between +9.8 to +21 o/oo . More than twenty samples ground water from 15 to 800 m deep have $\delta^{87}Sr$ values between +9.9 and +13.9 o/oo in contrast with five samples of Baltic Sea water collected in the vicinity of Äspö with $\delta^{87}Sr$ values between +0.2 and +0.4 o/oo -- only slightly larger than open ocean water ($\delta^{87}Sr$ = 0 o/oo). The 1.8-Ga host rock at Äspö is characterized by low Rb/Sr ratios, and a calculated mean $\delta^{87}Sr$ of approximately +2.5 o/oo demonstrates a lack of isotopic equilibrium between the ground water and the host granite at the bulk rock scale although

preferential mineral dissolution is possible. For example, biotite has extremely large $\delta^{87}Sr$ values, but studies of saline ground water in the Canadian Shield indicate that preferential reaction with plagioclase results in $\delta^{87}Sr$ that are typically smaller than the bulk-rock values. Calcite fracture fillings add further complexity to the Sr-isotope budget. Calcite fillings from depth between 363 and 612 m have $\delta^{87}Sr$ values between +4.7 and +9.9 o/oo whereas deeper samples (815 m) have smaller value of -3.0 to +0.6 o/oo coupled with an order of magnitude larger Sr concentrations.

$\delta^{13}C$ values in the calcite fissure fillings range between -25 and -3 o/oo and the $\delta^{18}O$ values range between +15 to +35 o/oo. The large range in $\delta^{13}C$ values is indicative of multiple sources for the carbon, including atmospheric, organic and methane derived carbon. The $\delta^{18}O$ signatures suggest mixing of meteoric and marine waters, but most of the calcites are precipitated from waters with $\delta^{18}O$ values similar to those of present-day ground water.

The stable isotope data from the calcite fissure fillings and the dissolved species suggest three different water layer at Äspö: (1) a shallow ground water (0-150 m) characterized by a mixture of meteoric water and minor proportions of Baltic Sea water, (2) an intermediate ground water (150 - 500 m) characterized by a mixture of marine and meteoric isotope signatures, and (3) a deep ground water body (>500m) which is highly saline with nonmarine signatures of the dissolved species. According to the seasonal variation of the isotopic signature (δD and $\delta^{18}O$) of the rain water the recharge of this water lens takes place during the autumn and the winter. In the intermediate water body, a substantial decrease in the $\delta^{34}S$ values of the dissolved sulphate indicates the addition of a component of a non-marine sulphur that could derive from the oxidation of sulphide minerals such as pyrite. Therefore, the sulphur and oxygen isotope data combined for that water suggest that it originates from an early injection of a highly oxygenated Baltic seawater after the latest ice recession in the area. The deep ground water body has a stable isotope assembly with overall typically nonmarine signatures. However, the spread in $\delta^{34}S$ values of the dissolved sulphate in combination with the sulphide sulphur signatures (Wallin, 1992) suggest that considerable bacterial sulphate reduction takes place in the upper part of this water body.

1. INTRODUCTION

This progress report summarises the results of a comprehensive stable (δD, $\delta^{18}O$, $\delta^{13}C$ and $\delta^{34}S$) and radiogenic (Sr) isotopic investigation of ground water and calcite fracture fillings at the SKB's Äspö Hard Rock Laboratory. The integration of these isotopic techniques, along with water quality data, provides a powerful approach for understanding the origin and evolution of the ground water and the hydrogenic minerals deposited in fractures. The fracture fillings mark the pathways of past fluid movement so an understanding of their genesis is particularly important for understanding the paleohydrogeology of the area. The utility in applying the multiple-isotope to ground water and fracture minerals derives from the fact that the different systems represent different processes. Oxygen and hydrogen isotopes in ground water at low temperatures are considered to be conservative with little modification by water-rock interaction. Hence, they reflect the values of water or waters recharged into the system. Dissolved carbon is derived largely through atmospheric input or by solution of CO_2 in the soil zone during infiltration. Among the stable isotopes, sulphur may exhibit the most complex behaviour because of its multiple valence states its amenability to bacterial fractionation. Strontium is a dissolved species geochemically analogous to calcium. The variability of strontium in ground water results solely from dissolution of or exchange with minerals during infiltration and along the flow paths. In addition to sourcing the ground water, O, C, and Sr provide important constraints on identifying the water from which the hydrogenic deposits precipitated. Sr isotopes do not fractionation with phases changes, and the fractionation of O isotopes can be readily calculated. If multiple but isotopically distinct waters are present, all of these systems are helpful in identifying mixing.

Äspö, an island situated on the Baltic coast in south-eastern Sweden (fig. 1), has been selected as a study site for evaluating the suitability of crystalline rock for hosting a nuclear waste repository. An underground laboratory (Äspö Hard Rock Laboratory--ÄHRL) is now being constructed at Äspö under a program initiated by the SKB (Swedish Nuclear Fuel and Waste Management Company) in 1986. This construction phase was preceded by detailed geologic site characterization studies to evaluate the capabilities of surface and drill-hole investigations to predict subsurface conditions (Wikberg and others, 1991). Extensive hydrologic studies were conducted in the pre-construction phase to establish a baseline for evaluating the impact of tunnelling on the local and regional ground-water systems. The final phase of the program will entail operation of the ÄHRL as an underground laboratory for the next decade.

A large number of scientists and research organisations are involved in this studies centered around the ÄHRL. SKB and DOE (U.S. Department of Energy) have several ongoing co-operative studies of the ground water, hydrogenic deposits, and bedrock at site. One of these studies is entitled "Task 3. Geochemical Investigations Using Stable and Radiogenic Isotopic Methods" (DOE/SKB Agreement, 1993) is focused on stable and radiogenic

isotope studies of the fracture filling minerals and the ground water. The results of investigations carried out during the first year of the program are summarized here. The geohydrologic system of any site being evaluated for a nuclear waste repository must be thoroughly understood.

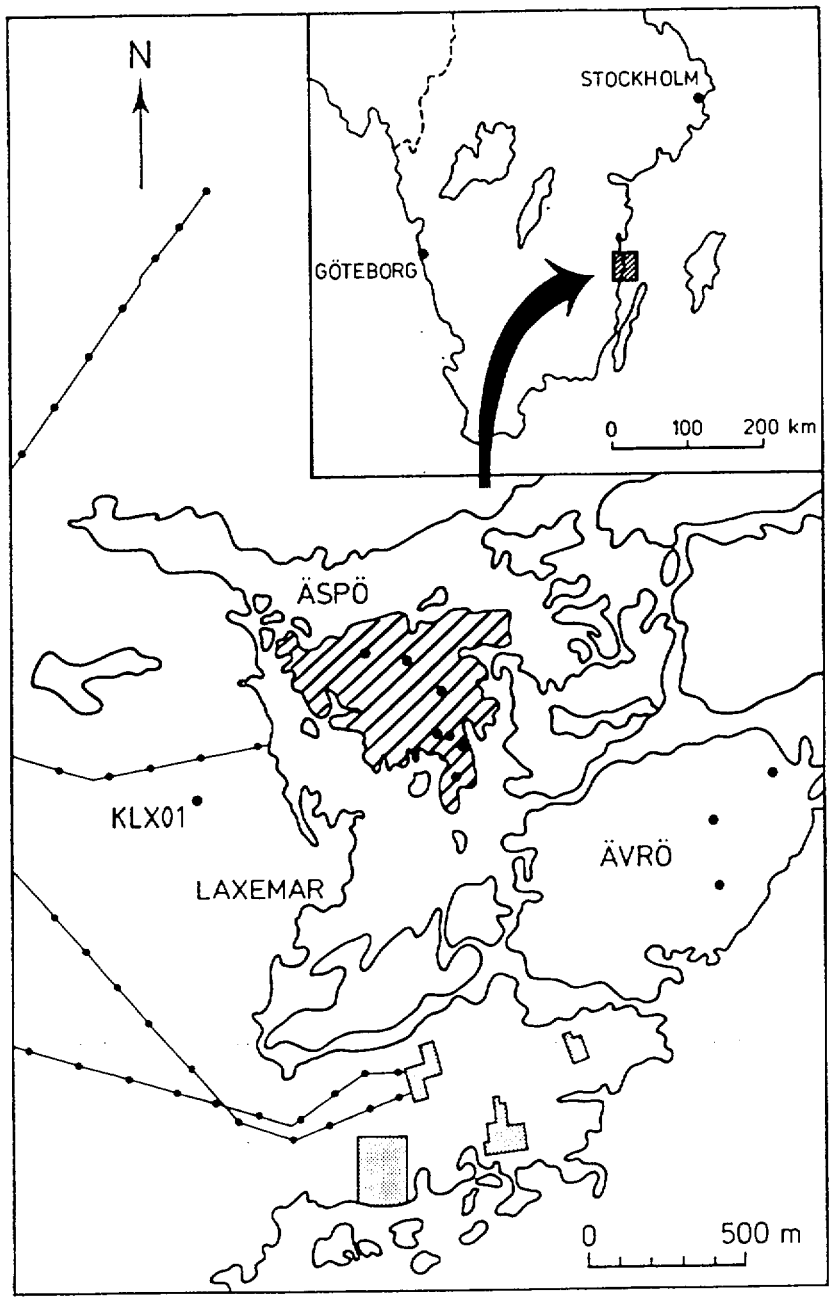

Figure 1. Map showing the location of the Äspö and Laxemar area.

Furthermore, the paleohydrology must be established in order to construct credible scenarios of possible future geohydrologic changes that could occur within the time frame of concern. The geohydrologic system at Äspö appears to be representative of crystalline rock terranes in the circum-Baltic region, but the origin and evolution of brackish-to-saline ground waters common to this region and the age and origin of hydrogenic fracture fillings are not yet fully understood. In order to attain a better understanding of the geohydrology at the site, and by inference similar areas in the region, a detailed sampling of fracture minerals as well as ground water has been made on a regular basis since August 1992 for this isotope study. Preliminary studies of the ground water chemistry suggest a very complicated history. However, the isotopic data obtained in this study demonstrate that it is possible to postulate mixing of marine, meteoric and "fossil" ground water end members to explain the complex ground water system at Äspö.

2. GEOLOGICAL SETTING, FRACTURES AND FRACTURE FILLINGS

The Precambrian basement rocks of the Äspö area are variably fractured crystalline rock of granodioritic to granitic composition with sheets or lenses of greenstone and metadacite. The granites are part of the serorogenic Småland-Värmland granites (ca 1.8 Ma) and the metavolcanic rocks are related to the Småland porphyries within the Svekokarelian belt.

The fracture frequency at Äspö is considered to be medium to high, whereas at Laxemar only 7 km towards the east it is low (Stråhle, 1989). The greenstones commonly have a higher fracture frequency than the granites. At least two different tectonic phases are recorded in the horizontal and subhorizontal fractures which are developed in the area. The fracture-filling mineralogy, which is similar at both sites (Stanfors, 1988), is dominated by calcite, hematite, Fe-oxyhydrite, chlorite, fluorite and minor proportions of sulphides. Calcite is by far the most common fracture minerals and is more abundant at Laxemar than at Äspö. Fluorite occurs primarily in subhorizontal fractures, which may be related to a specific event (Stanfors, 1988). The sulphides present are pyrite, chalcopyrite, and lesser amounts of galena. Pyrite, commonly present as well crystallised micron sized cubes, is the dominant sulphide. The pyrite cubes are usually found growing preferentially on the calcite in open fractures and appear to occur in greatest abundance between 400 to 500 m depth.

3. HYDROCHEMISTRY

The ground water at Äspö shows systematic compositional changes with depth (Smellie and Laaksoharju, 1992). Cl, Na, K, Ca, SO_4^{-2} and Br, increase progressively with depth and HCO_3^-, dissolved CO_2, Mg and Fe decrease with depth. The pH increases slightly with depth. The hydraulic conductivity is lower in the greenstones in comparison to the granite despite the fact that they

have a higher fracture frequency (Stråhle, 1989). The total water chemistry does not correlate with the different rock types that produce the water.

Stable isotopic data coupled with the concentrations of the dissolved components have suggested the presence of three distinct waters. These three water layers are: shallow water (0 - 150 m), intermediate water (150 - 400 m) and deep water (400 - 1000 m). This division is mainly based on the results from this study in combination with the previous isotopic studies at Laxemar (Wallin, 1990) and Äspö (Tullborg and Wallin, 1991).

4. METHODS

4.1. Sample Collections

In September 1992 and again in September 1993 ground water and fracture minerals were sampled. Ground water was collected from various depth in the wells HBH01, HBH02, KAS02, KAS03, KAS06, KAS07, KAS08, KAS09, KAS12, KAS13 as well as from the side wells (SA709 to SA2074) in the ÄHRL tunnel. Total dissolved inorganic carbon (TIC) from the ground water was sampled from filtered water for $\delta^{13}C$- and $\delta^{18}O$-analyses, and dissolved sulphate was precipitated for $\delta^{34}S$-analyses. Raw, unfiltered water samples were collected for $\delta^{87}Sr$-analyses and filtered and acidified in the laboratory prior to analysis. Rain water and sea water from the archipelago surrounding the island of Äspö were sampled as reference waters. Calcite fracture fillings were collected from open as well as filled fissures in the drill cores KAS02, KAS03 and KAS06. The granite and additional fracture minerals such as edidote, chlorite, flourite and pyrite were collected for bulk rock $\delta^{87}Sr$ and $\delta^{34}S$ analyses.

4.2. Analytical Work

4.2.1. $\delta^{13}C$ and $\delta^{18}O$ analyses

The calcite cement was extracted from the drill cores by use of a dental drill. The carbonate samples were reacted with 100% phosphoric acid in evacuated reaction vessels for 12 hours. Equilibrium of the reaction was made at a temperature of 25°C. Collection of CO_2 was done in a preparation line using liquid nitrogen to trap the gas. Excess water and other impurities was removed by freezing with a mixture of ethanol and dry ice. Cleaning with PbAc was used for some samples to free the CO_2 gas from any traces of H_2S gas generated from coexisting sulphides in the sample. A Finnigan MAT Delta E double inlet system mass spectrometer was used for the analyses. The analyses was performed at the Section of Biogeochemistry at the Department of Geology and Geochemistry at Stockholm University.

4.2.2. $\delta^{34}S$ *analyses*

Ground water was collected in acid-washed plastic containers. The samples were filtered and dissolved sulphate was precipitated as barium sulphate, carefully washed in distilled water, removed by decanting and dried. The preparation for the sulphur isotope analyses was made according to a technique proposed by (Sakai, 1982), where the sulphate was mixed with vanadium pentoxide (P_2O_5), silica (only small samples, pers com. Krouse, 1993) and pure copper and placed in a quartz glass boat and preheated in an oven at 450°C for 30 minutes. Then the sample was burned in an oven at 900°C for another 30 minutes. The SO_2 gas generated was collected in a pentane trap using liquid nitrogen to remove excess CO_2 gas. The SO_2 gas was the transferred to a sample vessel for analyses.

The extraction of the oxygen isotopes from the sulphate was made by the conventional reduction technique described by Rafter (1967), Mizutani, (1971) and Claypool (1980). The sample was mixed with graphite (C). The mixture was preheated for 10 minutes at 400°C to give a complete dehydration. The mixture was reduced at 1100°C and the CO_2 produced was then trapped by liquid nitrogen. Carbon monoxide gas (CO) formed during the reduction stage was converted by sparkling to CO_2.

Sulphur isotopes were determined with a Finnigan Mat Delta E, double inlet mass spectrometer at the Department of Geology and Geochemistry, Stockholm University, and at Energiteknikk at Kjeller, Oslo, Norway. The oxygen isotopes were run at the Laboratoire d´Hydrologie at de Geochimie isotopique at Universitee de Paris-Sud in Paris.

4.2.3 $\delta^{87}Sr$ *Analyses*

Strontium isotope analyses were completed in the laboratory of U.S. Geological Survey, Yucca Mountain Project Branch, Isotope and Geochemistry Section in Denver, Colorado. Water and carbonate samples were analysed on either a VG Isomass 54E or Finnigan MAT 262 mass spectrometer. The relative accuracy of the $^{87}Sr/^{86}Sr$ ratios is equal to or better than 0.01 percent of the values. This correspond to a 0.1 per mil in $\delta^{87}Sr$

5. RESULTS

The results from the $\delta^{13}C$ and $\delta^{18}O$ isotope analyses of the calcite fissure fillings and the $\delta^{34}S$ ground water isotope are presented in several plots. The strontium isotope analyses of the calcite fracture fillings and the analyses of the ground water are combined and presented in one figure. The $\delta^{13}C$ values are referenced to PDB (Pee Dee Formation Belemnite) standard, $\delta^{18}O$ to SMOW (Standard Mean Ocean Water), $\delta^{34}S$ to CDT (Canyon Diablo Troilite), and $\delta^{87}Sr$ to the value for modern sea water using USGS standard

EN-1 which is a *Tridacna* shell collected from Enewetok Lagoon in the western Pacific Ocean. Isotopic analyses of the water and the calcite fissure infillings are expressed in per mil (o/oo) deviations (δ values) form the appropriate standards listed above, where δ is defined as:

$$\delta R_{sample} = [(R_{sample}/R_{standard}) - 1\ ] * 1000$$

and R is either $^{13}C/^{12}C$, $^{18}O/^{16}O$, $^{34}S/^{32}S$, or $^{87}Sr/^{86}Sr$.

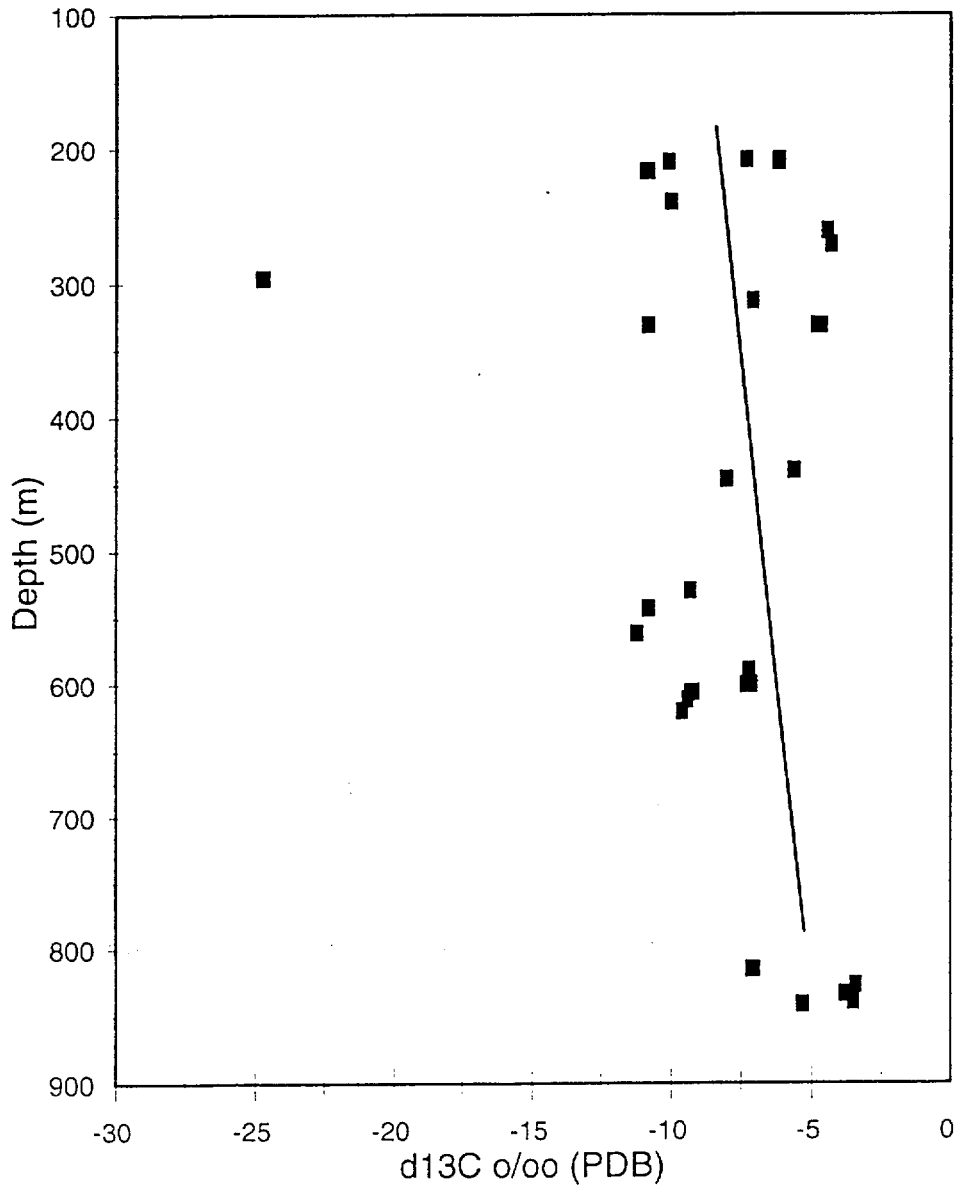

Figure 2. $\delta^{13}C$ values of calcite fracture fillings versus depth.

6. DISCUSSION

6.1. *FRACTURE MINERALS*

6.1.1. $\delta^{13}C$ *isotopes*

The $\delta^{13}C$ variation in the calcite fissure fillings display biogenic and typical atmospheric (-13 to -3 o/oo) values although one sample (-25 o/oo) and several in previous reports (Wallin, 1990; Tullborg and Wallin, 1992) show significantly lower values of -25 to -40 o/oo (fig 2).

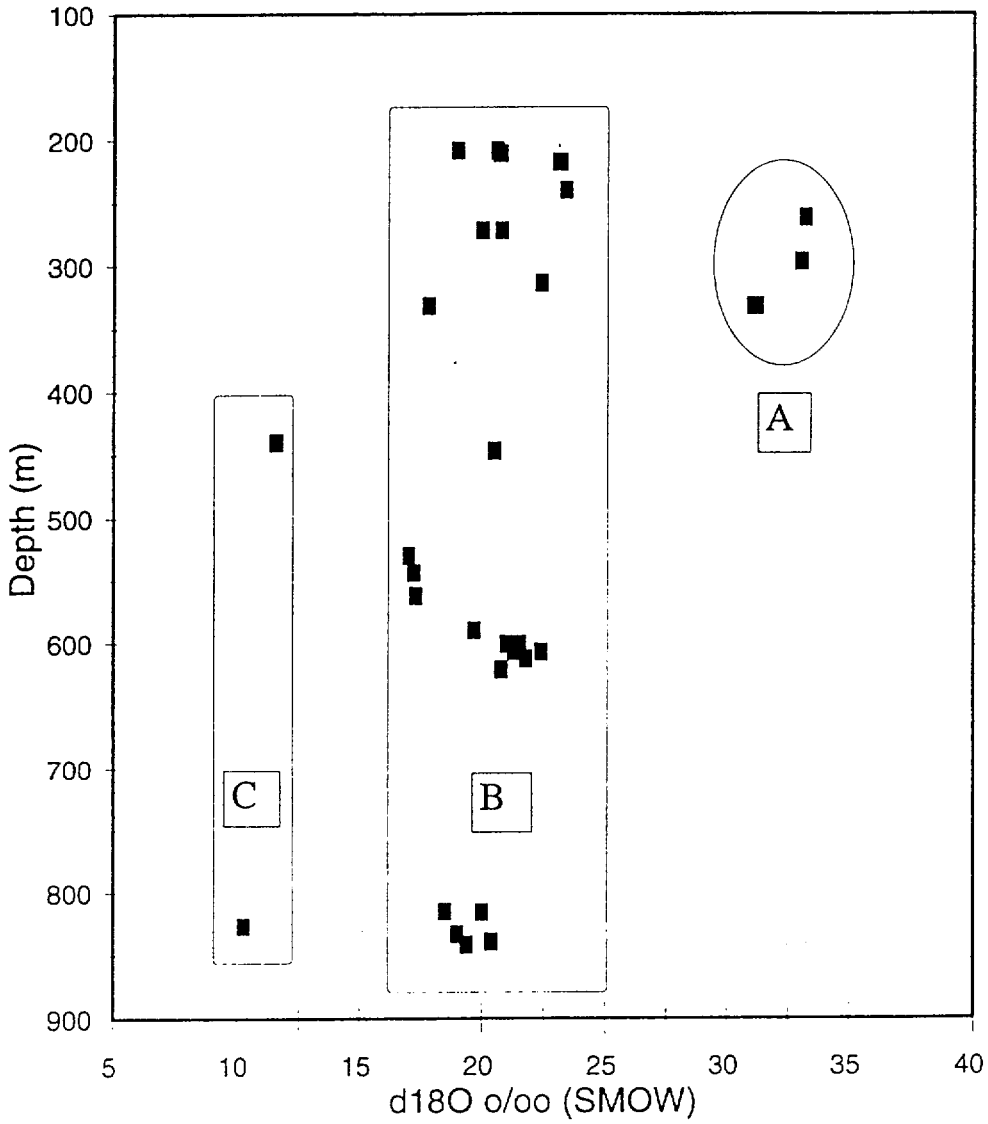

Figure 3. $\delta^{18}O$ values of calcite fracture fillings versus depth. 3 different groups appear A, B, and C. Group A show marine signatures and group B represent typical meteoric water precipitates. Group C may represent extremely depleted cold-water or high-latitude marine or meteoric waters.

Therefore, it seems most likely that the most of the calcites were precipitated from either meteoric or a mixture of meteoric and marine waters, which agrees with the $\delta^{18}O$ isotope evidence from the same carbonates. Some of the lower values reaching -12 and -13 o/oo , occur in some fractures together with flourite and may possibly be hydrothermal signatures as well. The slight increase in signature with depth (figure 2) may be attributed to a larger organic carbon input in the shallow waters. This is due to degradation of organic matter with CO_2 production which most likely is connected to the sulphate reduction which is taking place at Äspö (Wallin, 1992).

The extremely low $\delta^{13}C$ values which are observed in some carbonates are most likely attributed to a pure organic carbon source, with no influx of atmospheric signatures, presumably degradation of organic matter (Wallin, 1993; Banwart et al., 1993) or oxidation of deep seated (Arnorsen and Gunnlaugsson, 1985) and/or bacterially produced methane (Cheney and Jensen, 1965; Hathaway and Degens, 1965; Shultz and Calder, 1976). In either case there seem to be two major sources for the carbon observed in the calcite fissure fillings; one which is organic and one which is atmospheric.

6.1.2. $\delta^{18}O$ isotopes in calcites

The large spread in the $\delta^{18}O$ values (+10 to +35 o/oo) for the calcite fracture fillings indicate that these precipitated from isotopically distinct waters. Most of the $\delta^{18}O$ values resemble a typical meteoric signature, clustering around +17 to +23 o/oo . In fig. 3, these intermediate values are designated group B, whereas the higher values which are more characteristics of a marine signature are designated group A. Two samples have even lower values of about 10 to 11 o/oo and these are shown as group C. These lower signatures may be explained as precipitates from high latitude or cold climate waters. Similar lower values have previously been observed at Äspö (Tullborg and Wallin, 1992) and Laxemar (Wallin, 1990).

The group B isotopic signatures resemble values which are expected for calcites in equilibrium with the waters similar in $\delta^{18}O$ to those ground waters now observed at Äspö. To illustrate this, the calculated $\delta^{18}O$ values of calcite precipitates that would be in equilibrium with present-day Äspö ground waters are plotted versus depth in fig 4. It is clearly seen that the expected calcites that would be precipitated from present-day waters fall within the range of the group B calcites. Moreover, no calcite precipitates would be expected to form with the group A and C isotopic compositions from present-day ground-water $\delta^{18}O$ values. Hence, we may conclude that these carbonate precipitates with higher values around +33 and +35 o/oo in the calcite must therefore have been formed earlier from other water types, including marine and extremely $\delta^{18}O$ depleted waters such as glacial melt waters. Typical marine calcite precipitates usually fall in a narrow range of +30 to +31 o/oo . The group A calcite values at Äspö are slightly higher but are still representative of a marine water signature. Obviously, there is evidence of both marine and meteoric

$\delta^{18}O$ signatures as reported previously (Wallin, 1990; Tullborg and Wallin, 1992). Despite the low $\delta^{18}O$ values observed, a two end-member mixing of the calcites would hence be expected considering the that these two water types must have entered the basement at Äspö during the post-glacial time.

Another explanation for the narrow range in the $\delta^{18}O$ of the ground water at Äspö is that the saline water now observed are marine waters depleted in $\delta^{18}O$ due to mixing of glacial melt waters or cold climate precipitation. This phenomenon is well known from high latitudes and may very well be one explanation for the isotopically light waters (see section ISOTOPIC EVOLUTION OF THE PALEOBALTIC below).

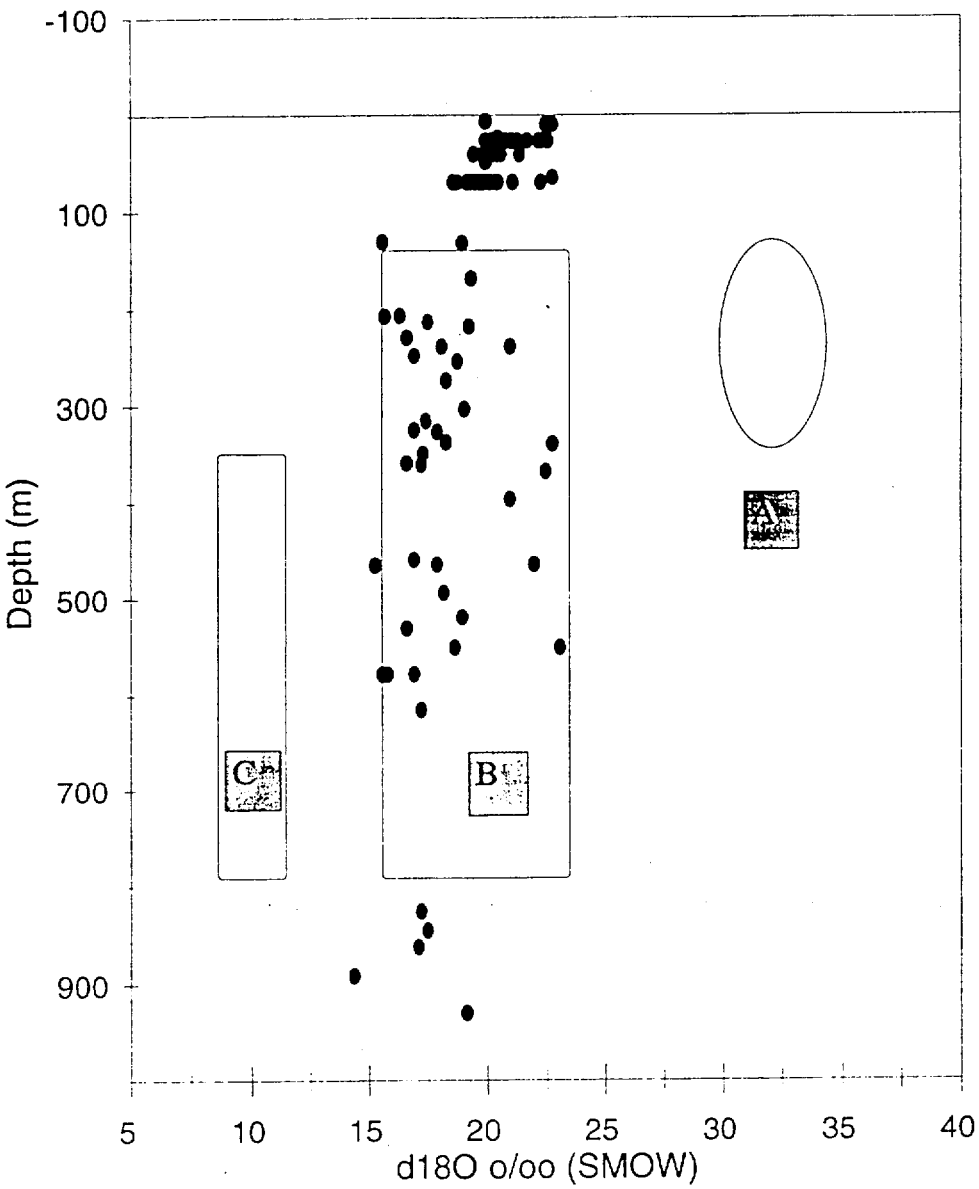

Figure 4. $\delta^{18}O$-values of possible precipitates from the present ground water. All values assemble in the group B from figure 3.

In figure 5, $\delta^{13}C$ is plotted versus $\delta^{18}O$. Except for two samples, the groups that are well distinguished on the basis of $\delta^{18}O$ (fig. 3) are not separated on the basis of $\delta^{13}C$. This is not surprising in view of the different sources and processes represented by these two isotopic systems. The two samples with high $\delta^{18}O$-values of +31 and +34 o/oo and low $\delta^{13}C$ values may have originated from an organic rich marine water, although more data is needed to further assess these possibilities.

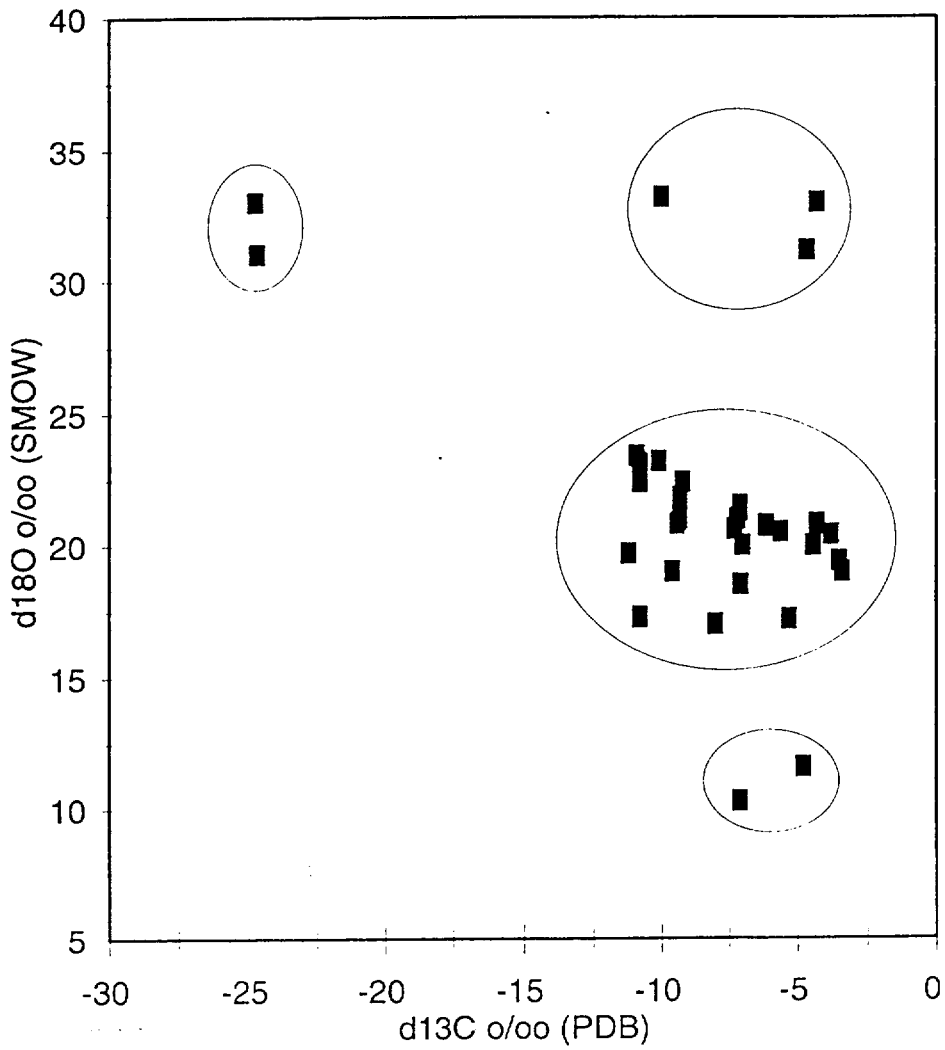

Figure 5. $\delta^{18}O$-values plotted versus $\delta^{13}C$ -values in calcite fracture fillings.

6.1.3. $\delta^{87}Sr$ *isotopes*

$\delta^{87}Sr$ values in the calcite precipitates ranges between -3.6 and +9.9 o/oo . Sr isotopes do not fractionate in nature so the $\delta^{87}Sr$ values of the calcites directly reflect those of the waters from when they precipitated. In addition, it is

interesting to note that at Äspö the concentration of Ca in the ground water correlate very well with the Sr concentration (fig. 6).

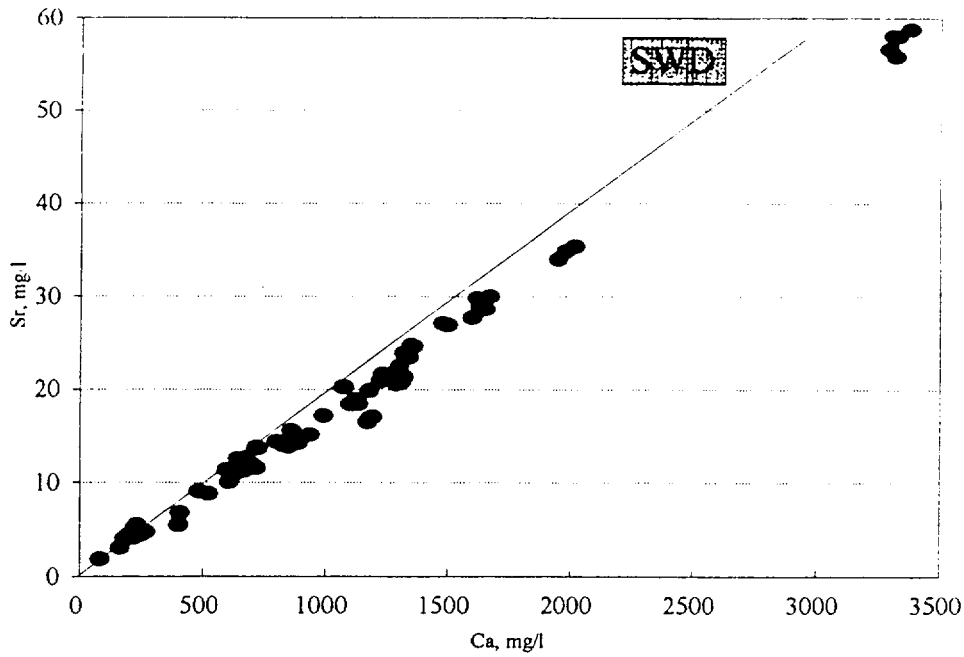

Figure 6. Sr versus Ca concentrations in the ground water.

Two groups of calcites are distinguished in fig. 7 where δ^{87}Sr values in the carbonates and the ground water are plotted versus depth. Five samples of calcites from 800 to 850 m have δ^{87}Sr values +0.6 and -3.6 o/oo. Calcites at shallower depths have a much larger range in δ^{87}Sr between -1.2 and +9.9 o/oo but most are greater than +3.3 o/oo. Only the two calcite samples with the largest δ^{87}Sr values of +9.8 and +9.9 o/oo could have precipitated from water isotopically similar to present-day ground water with δ^{87}Sr values between +9.9 and +13.9. Either the calcite fracture fillings were precipitated from an older and isotopically distinct ground water system or the source waters acquired less radiogenic Sr (low δ^{87}Sr) prior to precipitating the calcites. The range of δ^{87}Sr of the calcites is three times larger than the range in δ^{87}Sr of the ground-water and unlike the ground water values, the calcite δ^{87}Sr displays no systematic change with depth. These features suggest two possible scenarios. The first is that the calcites represent a long history of ground-water evolution with isotopically different ground waters at Äspö at different times in the past. The oxygen isotopic compositions of these multiple ground waters would have been similar to those of the modern ground water. The second scenario would call for localized water-rock interaction and acquisition of variable amounts of low δ^{87}Sr strontium prior to or during the precipitation of the calcites. The oxygen isotopic compositions of the water would be largely buffered from any significant change in this scenario.

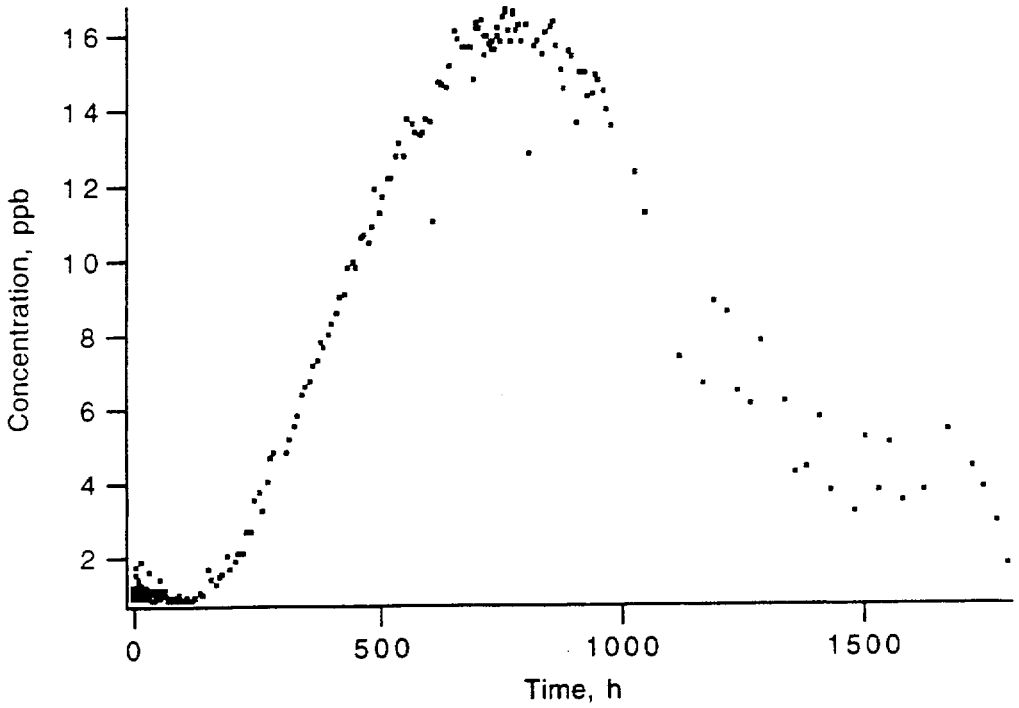

Figure 6. Breakthrough curve for Uranin for the total discharge in the withdrawal borehole, KAS06.

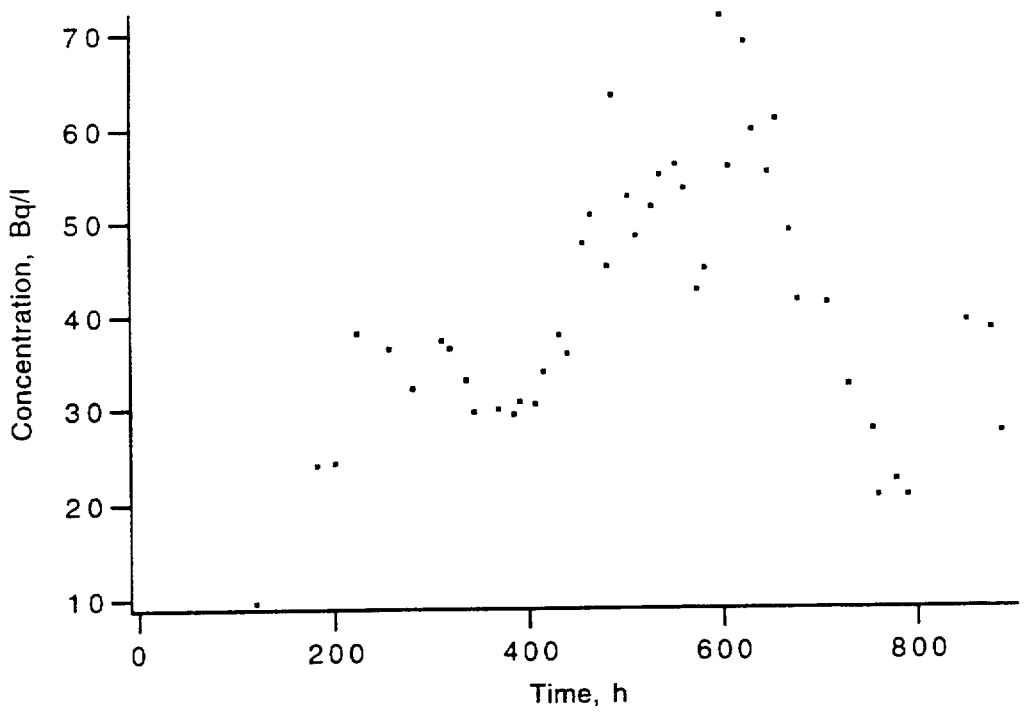

Figure 7. Breakthrough curve for Rhenium-186 for the total discharge in the withdrawal borehole, KAS06.

6 USE OF FIELD DATA TO OBTAIN MODEL PARAMETER VALUES

We have used field conductivity and transmissivity data to estimate the channel conductivity distributions for the fracture zones and for the rock mass in the model. Owing to lack of data the σ_C for the rock mass was assumed to be equal to the fracture zone value. The frequency of the fractures was used to estimate the specific flow wetted surface. Table 7 summarize the information from the Äspö Hard Rock Laboratory used and for which model parameter or purpose it has been used. No conditioning or parameter adjustments were made.

6.1 ESTIMATION OF THE CONDUCTIVITY DISTRIBUTION

One type of experimental data that can be used to obtain the parameter values in the model are the measured "conductivities" in boreholes. The mean conductivity of the rock mass was estimated to be $2.0 \cdot 10^{-10}$ m/s. This mean value is obtained from Rock Mass Unit 1 to 3 measured at site scale (Wikberg et al., 1991). A mean channel conductivity was given to each fracture zone from the transmissivity data in Table 1. A vast amount of conductivity data from the boreholes was obtained during the field measurements. From that data, with interest concentrated on the conductive points within the fracture zones, Figures 8 a,b,c and d below, were obtained. In the figures the distribution of the conductivity is shown and these data may be used in order to estimate the standard deviation in the channel conductance.

The borehole conductivity data measured in KAS02-KAS08 was given for three-meter packer intervals. The conductivity data from the borehole measurements was sorted and classified. Values belonging to different fracture zones were identified. The data points were sorted into specified conductivity ranges; we call it "bins". The conductivity data was classified into two different categories, "the best" and "good" data corresponding to the most reliable data and reliable data, based on the conductivity and flow measurements. Only these data were used and all other data values were discarded. In order to identify values which should be included, we used the available information obtained from geohydrological, injection and spinner tests (Wikberg et al., 1991).

After that, the reliable and the most reliable conductive points were identified, and with the aid of the Task Force data concerning the extension of the fracture zones, they were assigned to the appropriate zone. The conductivity frequency for some individual fracture zones is shown in Figures 8 a,b and c below. From these diagrams a σ_C for every individual zone was determined.

8a) Fracture zone EW-5

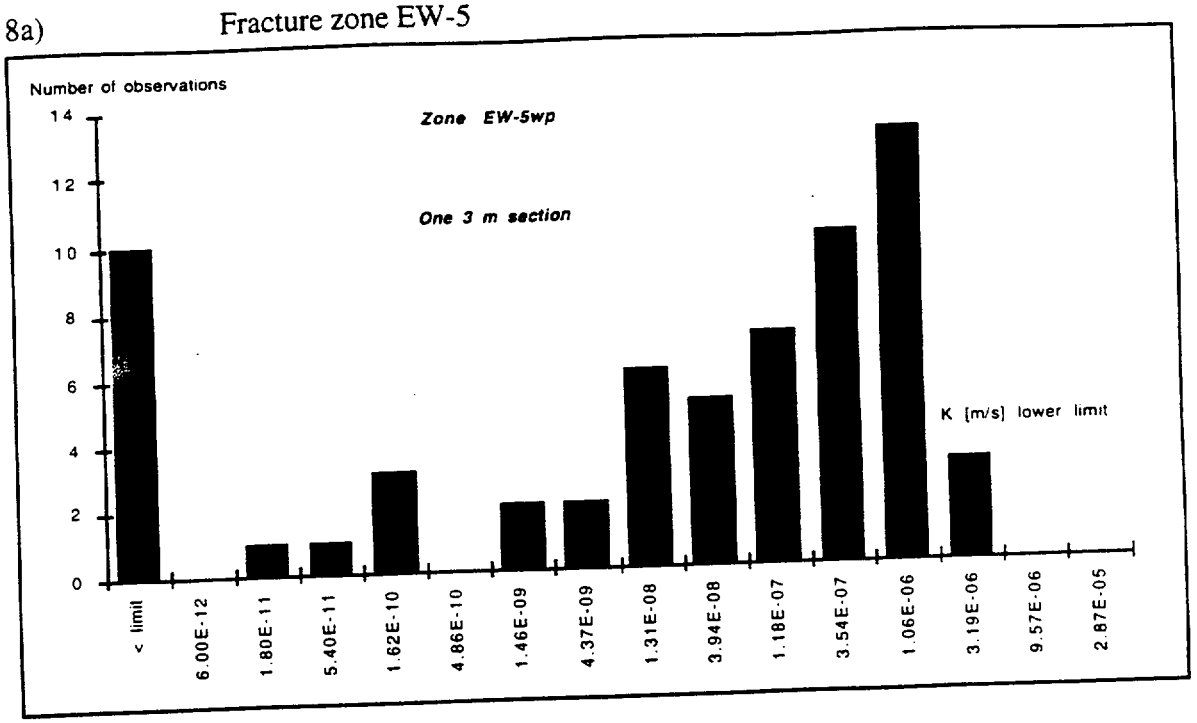

8b) Fracture zone NE-1

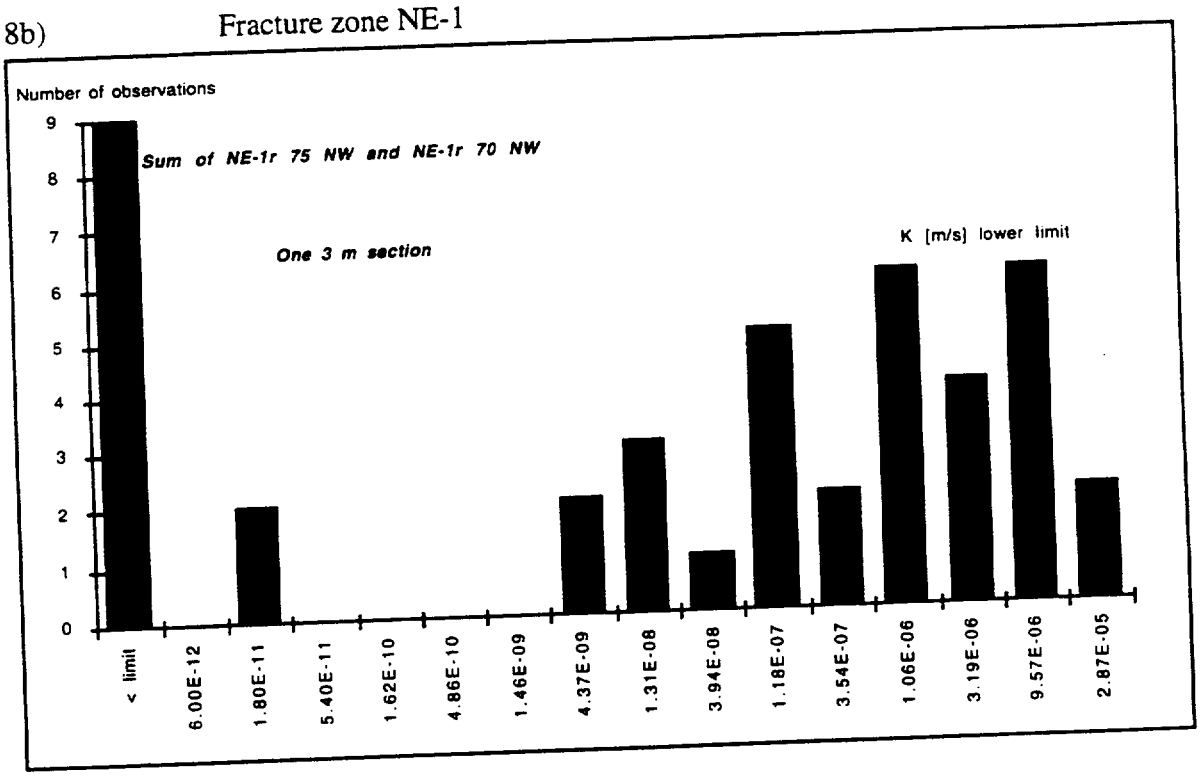

Figure 8a-b. The distribution of conductivities found in the fracture zones. Data is for the three meter sections. The first bar shows points below the detection limit within the fracture zones. The lower limit for each range is given.

8c) Fracture zones NNW-1 and NNW-2

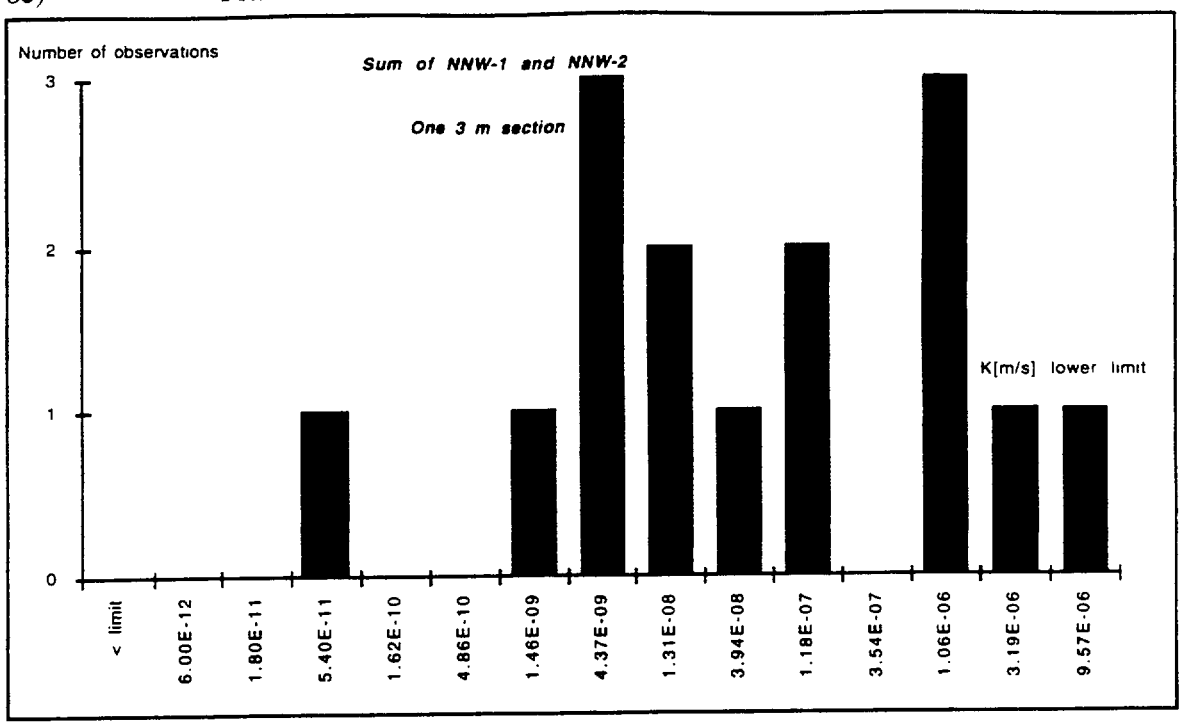

8d) All fracture zones included

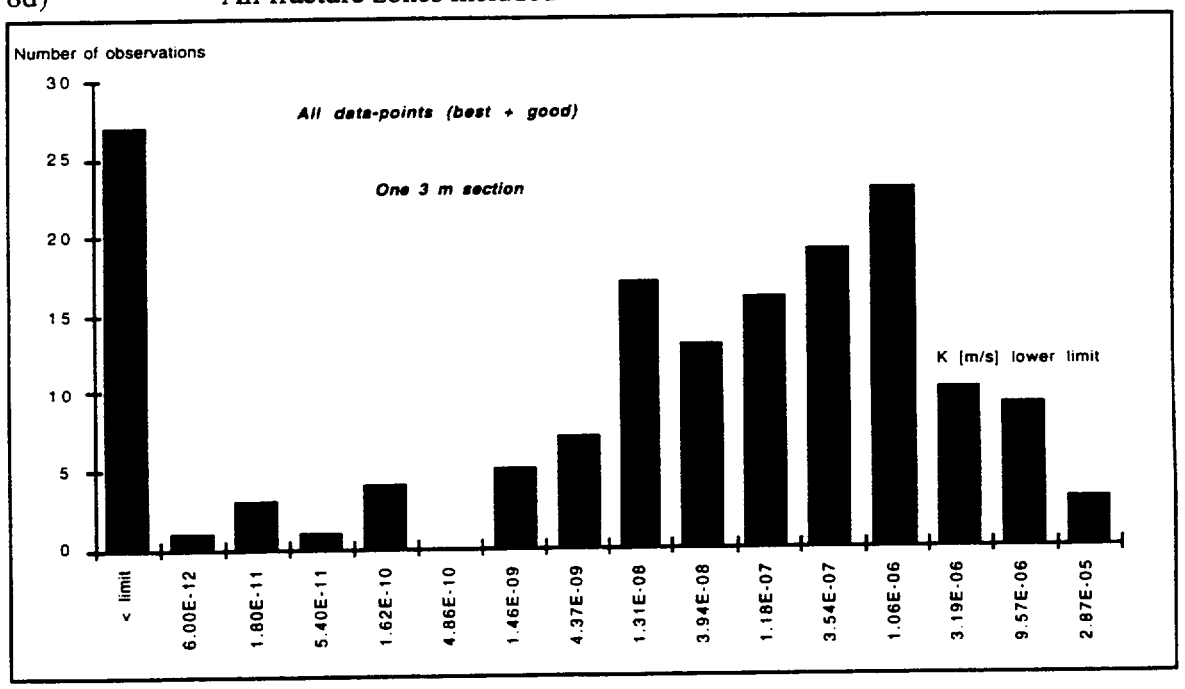

Figure 8c-d. The distribution of conductivities found in the fracture zones. Data is for the three meter sections. The first bar shows points below the detection limit within the fracture zones. The lower limit for each range is given.

The number of measurement data for each individual fracture zone is rather low, and from a model point of view it is more desirable to have a σ_C representing all the fracture zones, which may be obtained by using Figure 8d. An obvious drawback of gathering data from all the fracture zones into one plot is that if, for example, we consider a situation with two zones with fairly different mean conductivity and low individual σ_C, and we then put these conductivity distribution data together to get an overall mean value and a common σ_C for the two zones the σ_C will be misleadingly large. Based on these findings the σ_C used in the simulations was chosen to be 1.6, on the ^{10}log scale.

6.2 ESTIMATION OF THE FLOW WETTED SURFACE

It is important to know the flow wetted surface when the matrix diffusion into the rock matrix is to be modelled. How the flow wetted surface may be estimated from borehole data is shown in Appendix 2. From the borehole data shown in Figure 8d, it was found that the boreholes intersect a fracture about every 4 m. So, the borehole diameter, D_{bh} and the average distance between the channels, H, are the only known entities. As shown in the Appendix, if the channel width, W, is known then the flow wetted surface, a_R, may be obtained. However, W is not known unless independent observations have been made, e.g. in drifts and tunnels. Fortunately the specific flow wetted surface is not very sensitive to W provided $W >> D_{bh}$, and a_R may be obtained as:

$$a_R = \frac{\pi^2}{2H} \qquad (6)$$

A value of the flow wetted surface of 1.23 m^2/m^3 is obtained. In the Channel Network model the length of the channels were 20 m, this means that to match the flow wetted surface the width of the channel would be 82 m. This is not an unreasonable assumption since the fracture frequency in the fracture zone is rather high. The interpretation of this large width could be that each channel in the model is formed by several parallel channels with the same properties such that the total width is 82 m.

Table 7. Type of data used, source for the information and for what purpose or model parameter it has been used.

Type of used data	Reference	Model parameter/ Purpose
Fracture zone geometry	1,2,3	Locations and dimensions for fracture zones
Conductivity data from fracture zones obtained in boreholes (3 m sections)	4	σ_C for fracture zones
Spinner data	1	Confirm conductivity data
Transmissivity data for fracture zones	1	μ_O for fracture zones
Hydraulic conductivity for the rock mass	1	μ_O for rock mass
Conductivity data from fracture zones obtained in boreholes (3 m sections)	4	Specific flow wetted surface, a_R

1 = Wikberg et al., 1991
2 = SKB, 1993
3 = Rhén, personal communication, 1993
4 = SKB, 1992

7 RESULTS

The result from the pumping test is shown as the drawdown at various locations. The total flow into KAS06 is also calculated. The tracer test simulation results are presented by showing the flowpath for the solutes from injection to withdrawal and by breakthrough curves.

The simulations have been done by stochastic modelling and then the results become different for each realization. There was no attempt to perform any fitting or calibration in order to better match the results that were obtained in the experimental measurements at Äspö. Furthermore, there was no conditioning made in the modelling.

7.1 THE PUMPING TEST

We have simulated the steady state drawdown tests. Simulations of the transient pumping test were not performed. A base model was developed and used as a platform for the pumping test simulations. The ground for this base Äspö Channel Network Model was described in Chapter 4. Different types of boundary conditions were used. In the pumping-test simulations, this standard Äspö model, or versions of it with small modifications, was used so that different approaches could be tested.

Four types of pumping-test simulations were performed and they were carried out in order to study how the drawdown depends on various boundary conditions and parameters. Case 1 is carried out in order to study the influence of the infiltration rate, and case 2 to study the effect of a more conducting zone near the top surface of the model. A depth dependance for the conductivity has been observed in hydraulic conductivity field measurements and reported in KBS-3, (1983). Case 3 is performed in order to study the drawdown in the boreholes when we set the inflow at specified points in KAS06 equal to the obtained experimental inflow values for the same spots. Case 3 is also performed with a higher mean conductivity near the ground surface. In order to test the influence of a hydraulic head boundary condition on the surface case 4 was implemented. In each case at least ten runs have been carried out and they are summarized and listed below in Table 8. In order to make comparisons, case 2.a, intermediate infiltration and higher conductivity near the ground surface, was chosen to serve as a reference case.

The total inflow to KAS06 was also used in order to compare the simulation results with the experimental measurements. The experimentally determined inflow distribution is shown in Table 2, and the total mean inflow was around $71 \cdot 10^3$ m^3/year (Forsmark, 1992) during the experimental period.

Table 8. Boundary conditions and other conditions used in the simulations.

Case	BC on the top	BC in KAS06	Permeability near the top
1	**Infiltration rate**	**Head = -51.77 m**	
1.a	30 mm/year		Not modified
1.b	10 mm/year		Not modified
2	**Infiltration rate**	**Head = -51.77 m**	
2.a	30 mm/year		1000 times higher
2.b	10 mm/year		1000 times higher
2.c	150 mm/year		1000 times higher
3	**Infiltration rate**	**Flow in each section**	
3.a	30 mm/year		1000 times higher
3.b	30 mm/year		Not modified
4	**Constant head**	**Head = -51.77 m**	
4	Constant head		1000 times higher

7.1.1 Influence of the infiltration rate

The model version which was used in order to investigate the influence of the infiltration boundary condition was the Äspö base model (type of boundary conditions and permeability near the top as in case 1). The infiltration was evenly distributed over the ground surface. This means that the flux is constant through the upper model side. In the infiltration influence study we used three different rate values, 10, 30 and 150 mm/year.

From the simulations using an infiltration rate of 30 mm/year it can be seen that the obtained hydraulic-head results are higher than the experimental values. In Figure 9 the simulated drawdown versus distance squared for case 1.a together with the experimental values is shown. The distance is defined as that from a highly conductive location, within a packer interval, for the measurement borehole to the middle of the pumping hole, KAS06. In this plot the result for all the simulated boreholes is included. Points representing the simulated and the experimental values, for the same packer, may be seen right above each other.

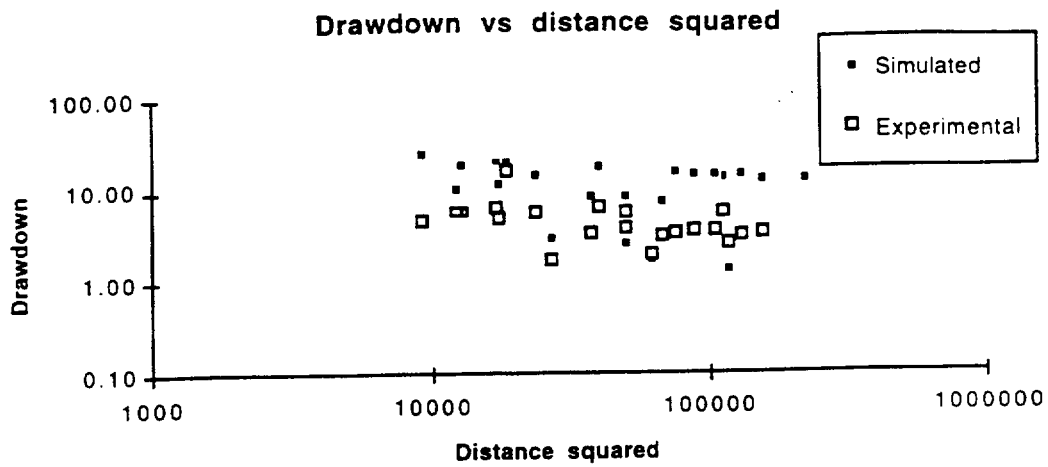

Figure 9. Case 1.a, performed with the unmodified standard Äspö model and with an infiltration rate of 30 mm/year.

The total inflow was overestimated by a factor of 1.66 compared to the field measurement in the simulation case, 1.a, with the intermediate infiltration rate.

In the calculations mentioned above, the infiltration rate was set to 30 mm/year. In order to investigate the influence of the infiltration rate, we have carried out runs with lower and considerable higher infiltration rates than this value. In the low infiltration case a rate of 10 mm/year was used. In Figure 10 the difference in drawdown versus the distance squared is shown. The difference in drawdown is here defined as the difference in hydraulic head, for each conductive measurement point, between the cases with low and intermediate infiltration rate. From the figure it can be seen that the difference is quite small, which means the change to the lower infiltration rate has no large influence on the result but it does, however, result in somewhat larger hydraulic head values and the deviation from the experimental drawdown values increases.

In the simulation with the lower infiltration rate the total inflow was overestimated by a factor of 1.63, and also just somewhat less than in the intermediate inflow case.

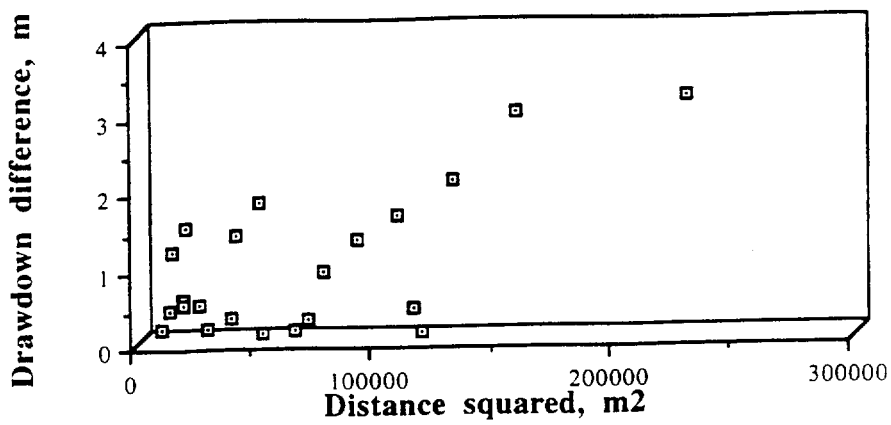

Figure 10. The drawdown difference between the cases 1.b and 1.a, with 10 and 30 mm/year infiltration rate, respectively, versus the distance to KAS06 squared.

When a higher infiltration rate (150 mm/year) was used in the simulations, locations on the ground with low conductivity get an unrealistically high hydraulic head. This is caused by the fact that the infiltration rate is constantly and evenly spread out over the ground surface and when the infiltration is then "forced" to penetrate the surface at the low conducting areas a high hydraulic head develops. The total inflow was 1.8 times higher than in the field experiment with the high infiltration rate case.

According to experimental measurements the hydraulic conductivity is generally higher near the surface (KBS 3, 1983). The conductivity near the surface may, compared to locations at large depths, be considerably higher. For these reasons a layer with high conductivity near the ground surface was used in the next set of simulations.

7.1.2 Effect of higher conductivity on the upper model layers

The model was modified slightly in order to investigate the influence of a layer with higher conductivity near the ground surface. The modification was that the channels near the surface were given a mean conductivity three orders of magnitudes higher than the same channels used in the basic model. In these calculations, here called case 2, the infiltration boundary condition was used and the rate was assigned the same three values as above; 10, 30 and 150 mm/year. The infiltration was evenly distributed over the ground, which means that the flux is constant through the upper model side.

This approach is in line with the conductivity distributions that have been obtained in some field studies as mentioned above. The simulated hydraulic head values for case 2 are in better agreement with the experimental values compared to case 1.a. The case 2.a with an infiltration rate of 30 mm/year was chosen to serve as a reference for the other sets of

simulations. Figure 11 shows case 2.a result as the drawdown at various measuring points versus the distance to KAS06 squared. The experimental values are also included for comparison.

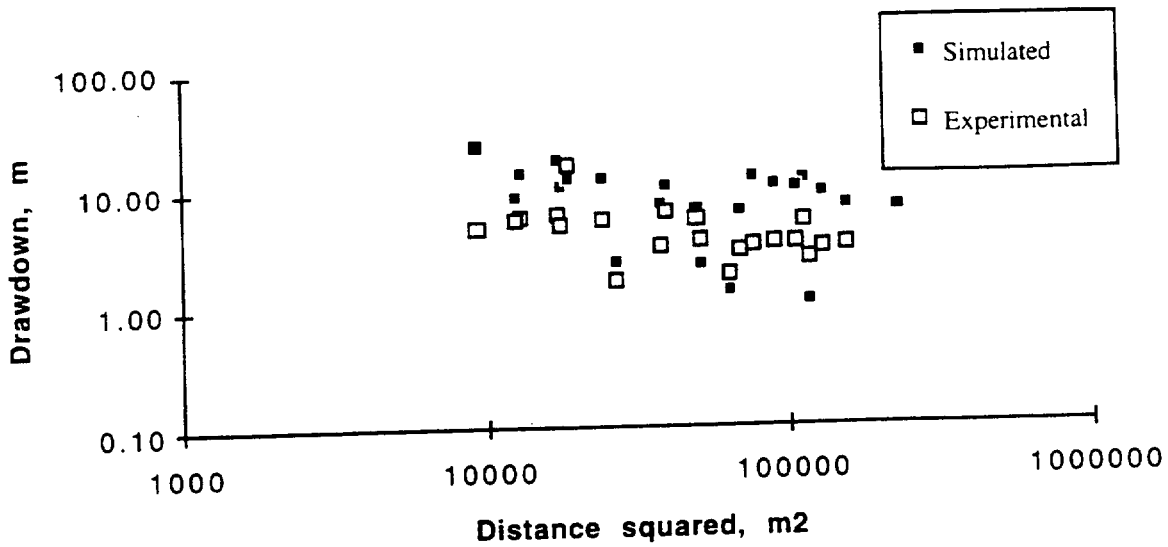

Figure 11. The drawdown at the packer intervals for the pumping experiment and the case 2.a simulation result. In this case, a higher conductivity on the ground surface and an infiltration rate of 30 mm/year were used. This case is used as a reference case for the other simulations.

It may be hard to distinguish the different points in the plot above, therefore the results for each particular borehole are also shown in Figure 12. In the plots the figures on the x-axis correspond to the packer intervals. For some holes, the results from the simulations and the experiment are in some agreement.

Generally, the drawdown results approach the experimentally measured values with an increasing infiltration rate, at least in the range we have been studying. That is, the highest infiltration rate used gave the best agreement between observed and simulated drawdown. On the other hand the overestimation of the total inflow increases with the infiltration rate. The total inflow over-estimation factors are 1.76, 1.77 and 1.82 for the low, intermediate and the high infiltration rate case respectively.

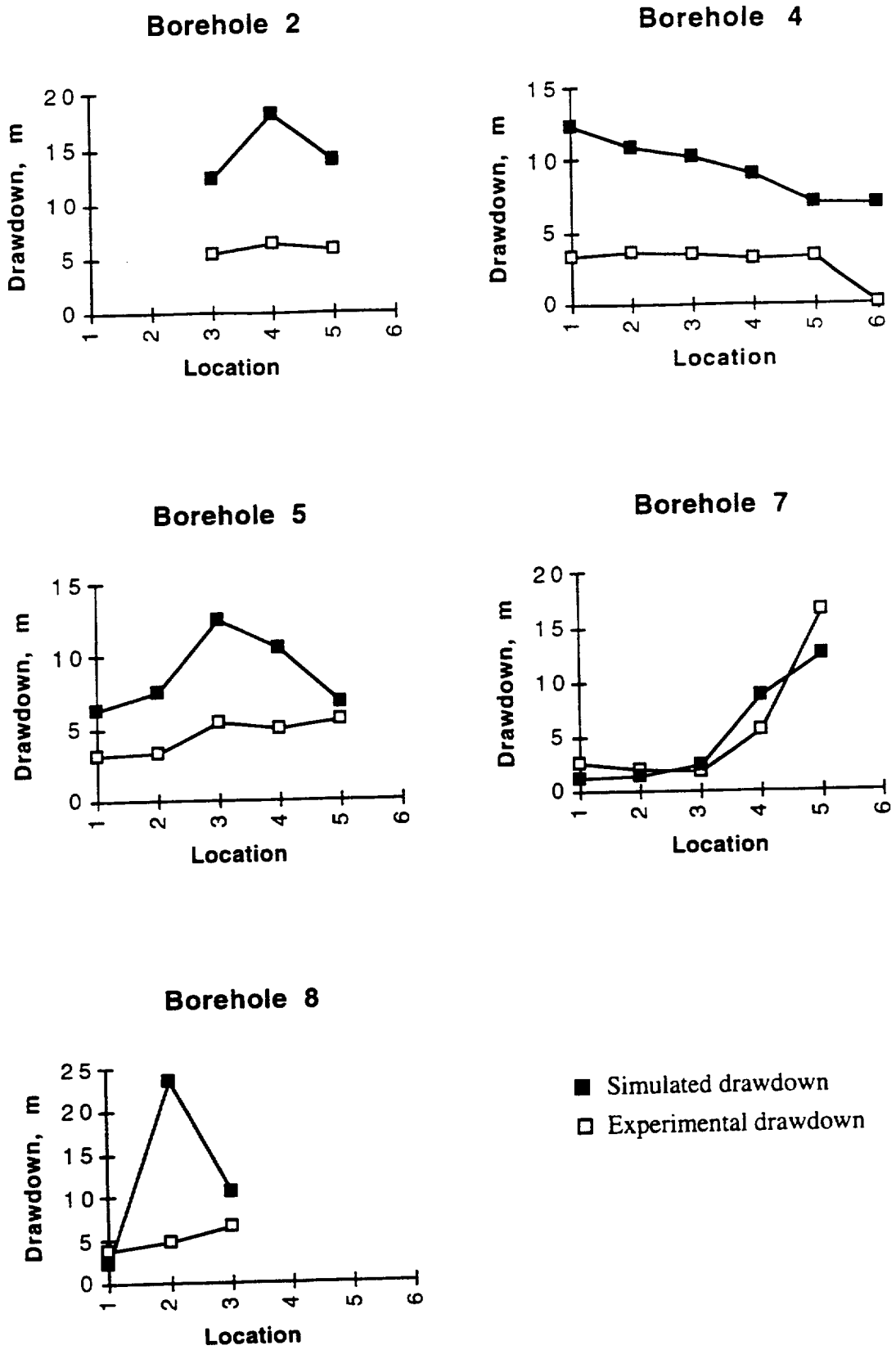

Figure 12. The steady-state drawdown in all the individual simulated boreholes. The simulation is performed under case 2 conditions, high conductivity near the ground surface and an infiltration rate of 30 mm/year.

7.1.3 Determined inflow to KAS06

Simulations with the inflow determined, at each location, from the field experiment have also been performed. The location of the inflows and their relative magnitude is shown in Table 2. The used infiltration rate through the top of the model was 30 mm/year. Both simulations with the standard model and the modified model with higher permeability near the surface were carried out. In fact, the results from case 3.a with determined inflow, high mean conductivity on the ground and an infiltration of 30 mm/year were closest to the experimental results. The drawdown from this case is shown in Figure 13. The other case with no modification of the surface layer was the second closest. In these two cases it is of course no use to compare the inflow to KAS06 with the experiment, because it was set equal to the field value.

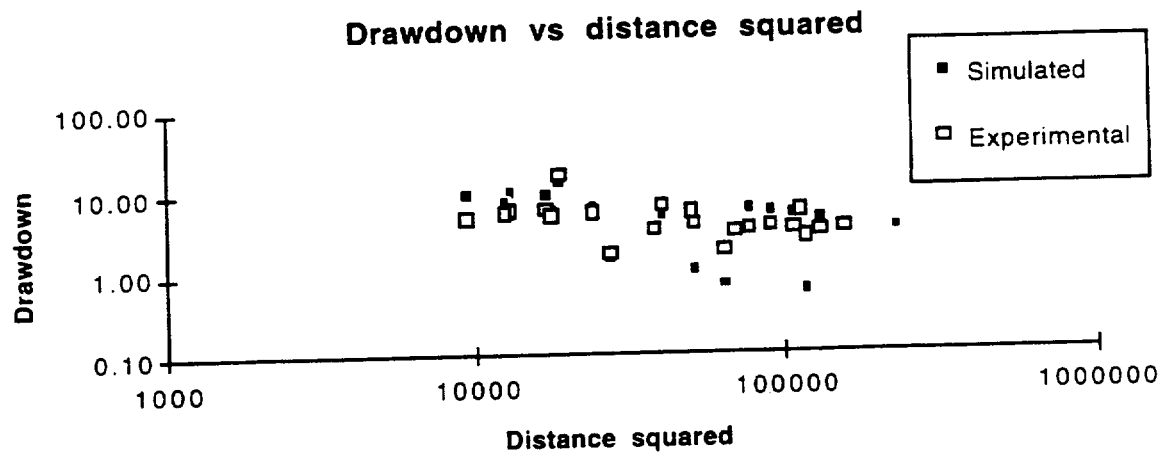

Figure 13. Drawdown versus the distance from KAS06 squared. Case 3.a, determined inflow values set to the experimentally obtained values. High permeability through the ground and an infiltration rate of 30 mm/year.

7.1.4 Hydraulic head boundary condition on the top surface

The pressure field will be influenced by the boundary condition. The boundary condition on the surface used in the previous cases, specified infiltration, will cause a fairly high head on locations with low conductivity. The pressure field also depends on the infiltration rate. The magnitude of the infiltration may also be quite difficult to determine correctly. Therefore, we have tested another boundary condition namely a specified head on the ground surface. In this simulation the conductivity of the top level was increased.

The drawdown result was approximately of the same order as the reference case with infiltration boundary condition (30 mm/year). The total flow into KAS06 was larger than the experimental value by a factor 1.85.

The flow field for one realization is shown in Figure 14. The flow field is shown by a surface showing a constant value of the flow rate. Here, a surface with a fairly high constant flow rate is shown and surfaces with lower flow rate values are made transparence. It may be seen that the fracture zones serve as the major conduits.

The pressure field around the withdrawal hole KAS06 is shown in Figure 16. The blue colour indicates the low hydraulic head at points where the connections between the pumping hole and the fracture zones are good.

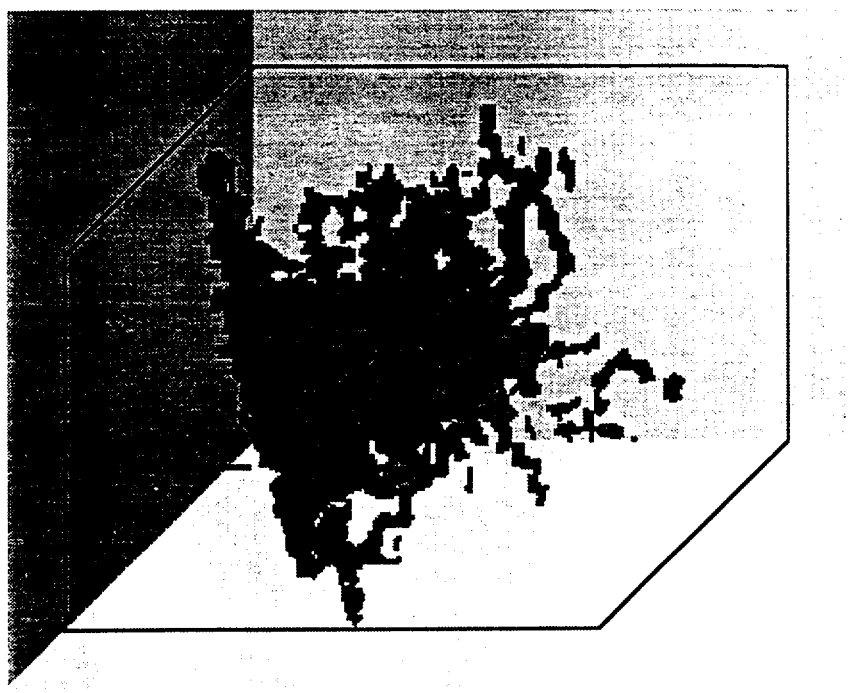

Figure 14. The simulated flow field.

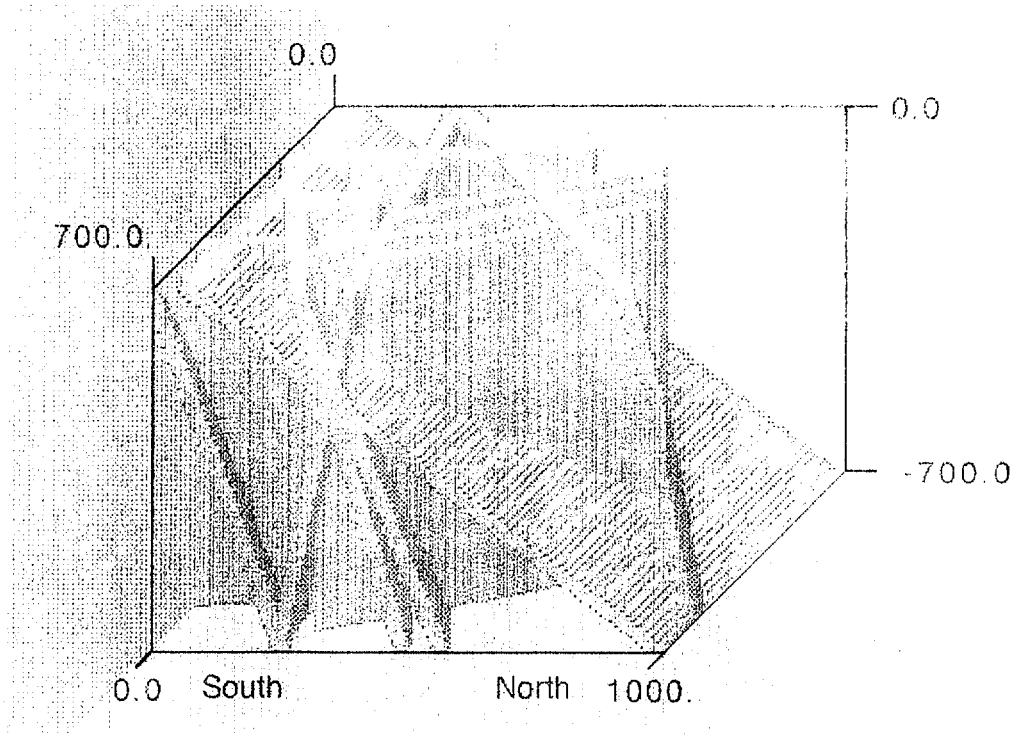

Figure 15. The modeled major fracture zones at Äspö.

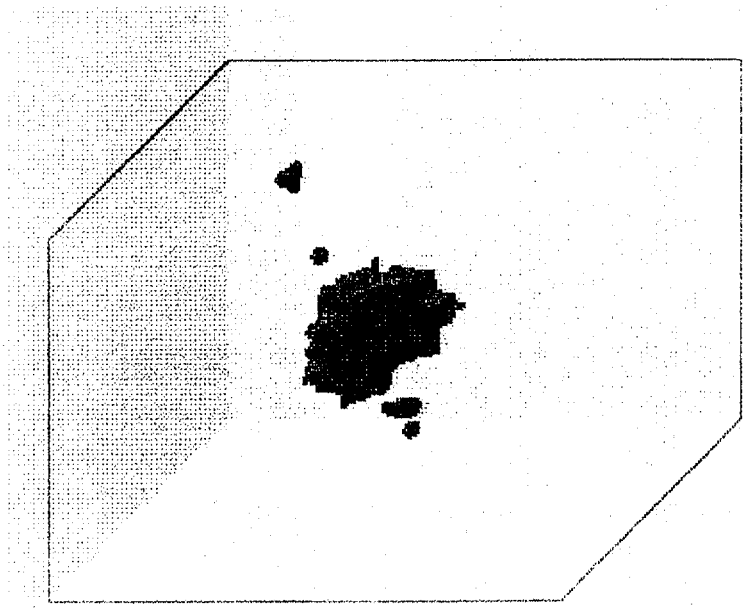

Figure 16. The simulated pressure field around the withdrawal hole KAS06.

7.2 THE TRACER TESTS

The simulations of the tracer test have been carried out in the same 3-D grid used for the pumping test simulations. The pressure field from the case with a higher mean conductivity at the upper part of the model and an infiltration rate of 30 mm/year, has been used to perform all the tracer tests. Furthermore, as boundary condition in the withdrawal hole the determined inflow approach was used to get flow rates more like the ones found in the experiment. The standard deviation in channel conductance is 1.6 for channels within the fracture zones, the rock mass and the upper model layers. In the tracer test simulations we have assumed the flow porosity for the fracture zones to be 0.001 and 0.0001 for the rock mass. It is further assumed that the volume of a channel is proportional to the cubic root of its conductance. This is the common cubic law assumption. In order to carry out the tracer test simulations, a particle following technique has been used. The tracers have been treated as non-sorbing and we have included diffusion in the rock matrix. The diffusion for the solutes is determined by the group of constants, $LW(K_d\rho_p D_e)^{0.5}$ in Equations 4 and 5, where 2LW is the flow wetted surface for one channel, $K_d\rho_p$ is equal to the pore porosity, ε_p, for non-sorbing solutes and D_e is the effective diffusivity. The flow wetted surface was obtained from the borehole data. In Appendix 2 we discuss how LW and the flow wetted surface can be estimated. $K_d\rho_p$ which for the non-sorbing tracers is equal to the rock porosity ε_p is assumed to be 0.003 and D_e is $3.15 \cdot 10^{-6}$ m^2/year. The group of constants $LW(K_d\rho_p D_e)^{0.5}$ will be called G in the following.

The injections of tracers in the field experiment were carried out in two ways; decaying pulse injections and intermittent decaying pulse injections. This has been considered in the simulations, so our simulated tracers are injected in a similar way. In the simulations the intermittent injection was modelled as several pulse injections at times corresponding to the times used in the experiment. The schedule for the cases with intermittent injection is shown in Figure 17.

The results of the simulated tracer tests are studied by means of the breakthrough curves and by pathway tracking for the tracers from the injection to the withdrawal hole. The experimental breakthrough curves at the Äspö site are displayed in section 5.2 for the total discharge.

We do not intend to fit the simulation results to the experimentally observed curves. We will, however, explore how the parameter values affect the breakthrough. We will also discuss the impact of some of the main assumptions.

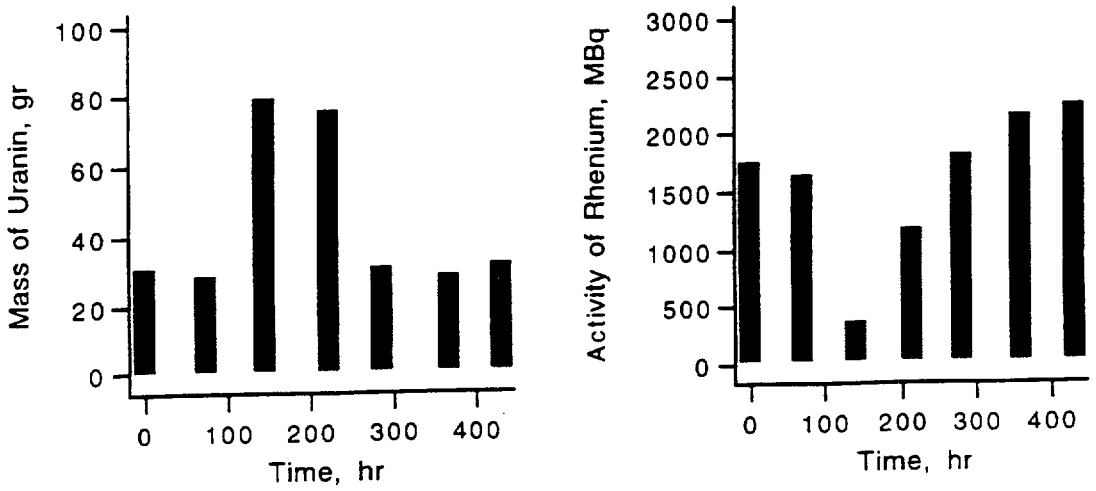

Figure 17. The modelled injection schedule for the tracer tests with intermittent injection. Left: injection in KAS12-2. Right: injection in KAS08-1.

The experimental and simulated local water flows at the injection points are shown in Table 9. For this realization there are some deviations between the field and model values.

Table 9. The experimental and simulated local water flows at the injection points.

Borehole	Packer interval	Experimental m^3/year	Simulated m^3/year
KAS02	4	1.10	87.95
KAS05	3	4.73	23.19
KAS07	4	9.59	341.24
KAS08	1	24.85	14.34
KAS08	3	11.04	38.85
KAS12	2	55.71	21.93

7.2.1 The pathways for the solutes

In several simulations, the pathways followed by the particles were displayed in a 3D plot. From this kind of plot it is possible to determine the fracture zones through which the solute has travelled. Pathways for the solute injected in KAS12 from injection to detection in the withdrawal hole KAS06 are shown in the Figure 18. In our simulation the solutes choose two main paths. According to our simulations most of the solutes travel through the zones NNW-4, EW-1 and NNW-2. That is the path to the right in Figure 18. The schematic main path for all the simulated tracer tests are shown in Table 10.

Table 10. The simulated main path for the tracers from injection to detection in KAS06.

KAS02-4	NNW-1,W	KAS06				
KAS05-3	EW-5,W	NNW-2,W	KAS06			
KAS07-4	EW-5,W	NNW-1,W	KAS06			
KAS08-1	EW-1,W	NNW-2,W	KAS06			
KAS08-3	NNW-2,W	KAS06				
KAS12-2	NNW-4,W	EW-1,W	NNW-2,W	KAS06		

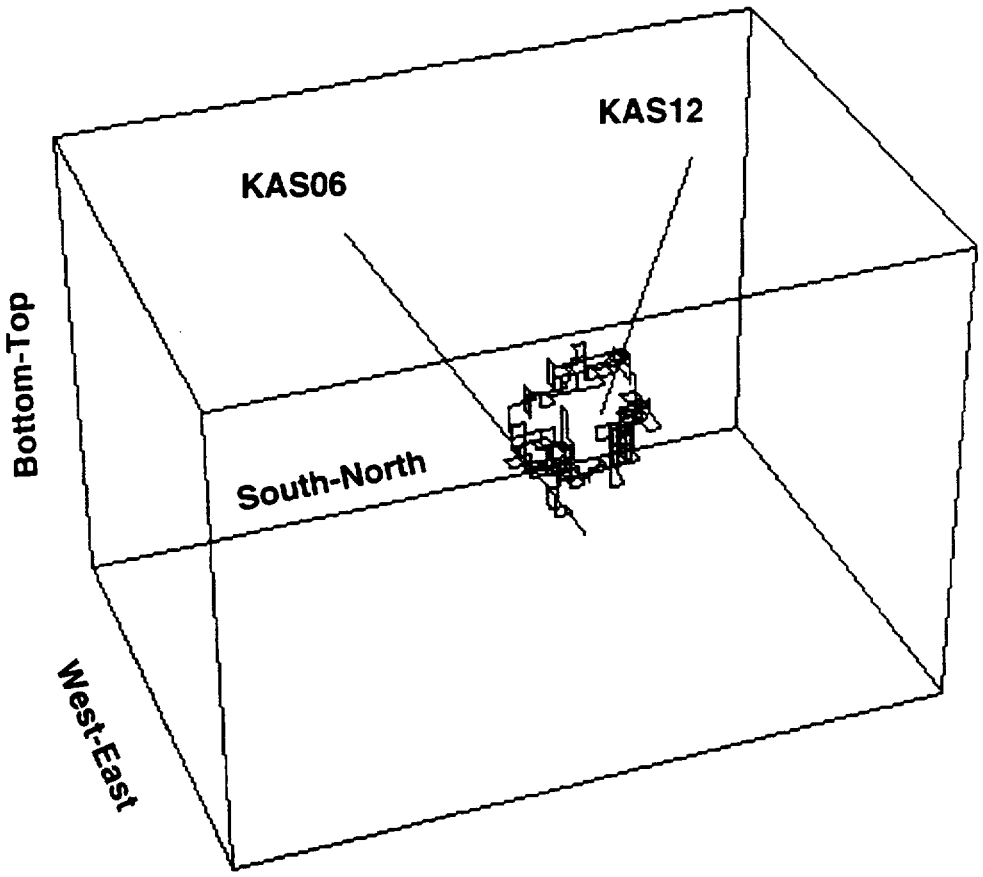

Figure 18. The pathways for the solutes from KAS12 to KAS06.

7.2.2 Breakthrough curves

Breakthrough curves for four non-sorbing tracers, three short-lived radioactive tracers and one fluorescent dye, are simulated for the six different tracer tests.

Simulated breakthrough curves for the tracer test with injection in KAS12-2.

This tracer test resulted in clear experimental detections which is shown in Figure 6. For simulation of tracer tests a reasonable estimation of the flow wetted surface is important though we assume that also the non-sorbing solutes will diffuse into the rock matrix. The magnitude of the flow wetted surface will then be controlling the degree of diffusion. How the flow wetted surface may be estimated is described in section 6.2 and Appendix 2. The group G may be determined from the previously obtained data from the borehole measurements and laboratory data. The latter from this site is not known and thus may be uncertain. There are no data on the flow porosity and we assign a value taken from previous experience from the Stripa experiment. If ε_p is taken to be 0.003 and D_e is

$3.15 \cdot 10^{-6}$ m²/year then the value of the group G is about 0.16. The flow porosity, ε_p, is not known, so a value of 0.0001 is assumed.

The simulated breakthrough curves from injection of Uranin in KAS12-2, using these values for G and ε_p, is shown in Figure 19. It is shown together with the experimental curve. A reasonable good agreement is obtained, considering that no fitting at all has been done and that much of the data is estimated and not site specific. The amount of recovered tracer is larger in the simulation than that in the experimental test. The tracer recovery during the observation times (1 794 hours) for the simulated curve is about 79 %. The experimental recovery was 38 %. A simulation with flow porosity of 0.001 was also made and the results are shown in Figure 20. This result shows that the results are quite sensitive to some of the parameters where data are very uncertain and probably variable.

If no diffusion into the rock matrix in the simulation of this tracer experiment is used the concentration gets somewhat higher and the time for the main peak to arrive is approximately the same. This implies that the effect of the diffusion is still underestimated in our calculations. A lot of crushed material in the fracture zones would result in a larger flow wetted surface which will increase the effect of the diffusion.

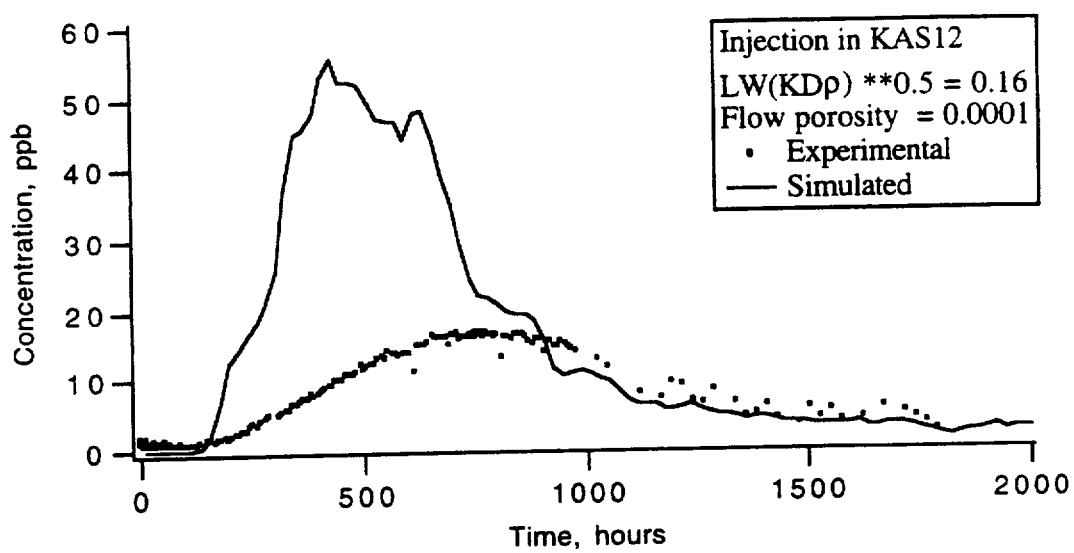

Figure 19. Simulated and experimental curves for Uranin from KAS12-2. In the simulated case, the value 0.16 is used for the product $LW(K_d\rho_p D_e)^{0.5}$ and 0.0001 for the flow porosity.

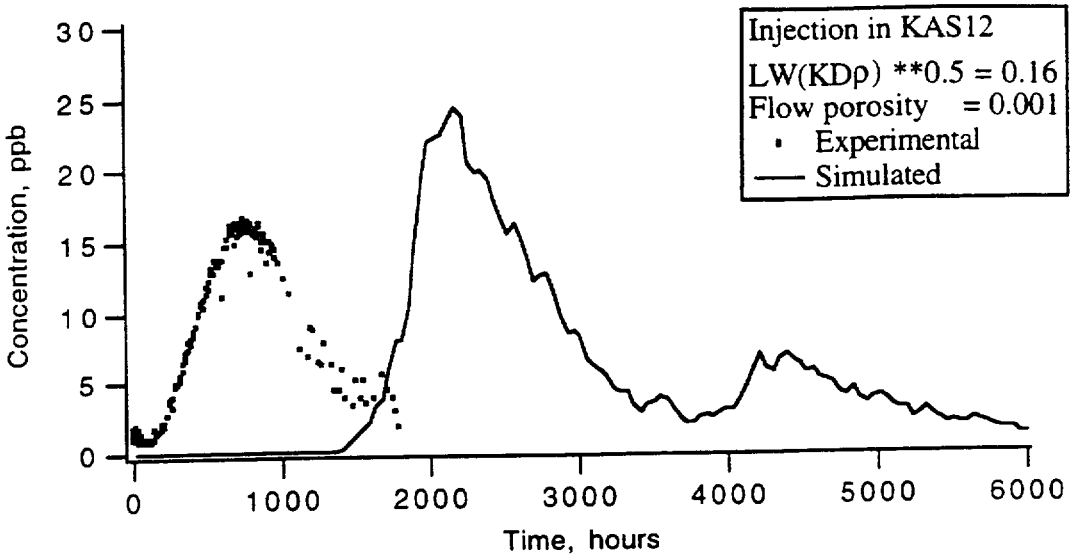

Figure 20. Simulated and experimental curves for Uranin from KAS12-2. In the simulated case, the value 0.16 is used for the product $LW(K_d\rho_p D_e)^{0.5}$ and 0.001 for the flow porosity.

Simulated breakthrough curves for the tracer test with injection in KAS08-1.

Rhenium was injected in KAS08 packer section 1. The injection was carried out with an intermittent pulse injection and the total time of injection was 431 hours. The total time for the test was 890 hours. The test gave a low recovery of tracer, a fairly broad peak and the time for the first tracers to arrive at the detection hole was around 200 hours.

We have simulated this test with the combination of parameters as in the simulation of the Uranin tracer test with injection in KAS12-2, i.e. $\varepsilon = 0.0001$ and $G = 0.16$. The result for this simulation is shown in Figure 21. In our simulation with the above mentioned combination of parameters we obtained a recovery of 77 %. This figure is very high compared with the experimental one, which was about 2-3 % during the observation time. The time for the first tracers to arrive was around 80 hours. The breakthrough curve simulated using a flow porosity of 0.001 is shown in Figure 22.

The low recovery in the field experiment may be due to that the test was terminated after a short time (890 hours) so that the main mass of the tracers never reached the withdrawal borehole. There may also be a loss of tracer by some irreversible process. This will be discussed in more detail in the next section.

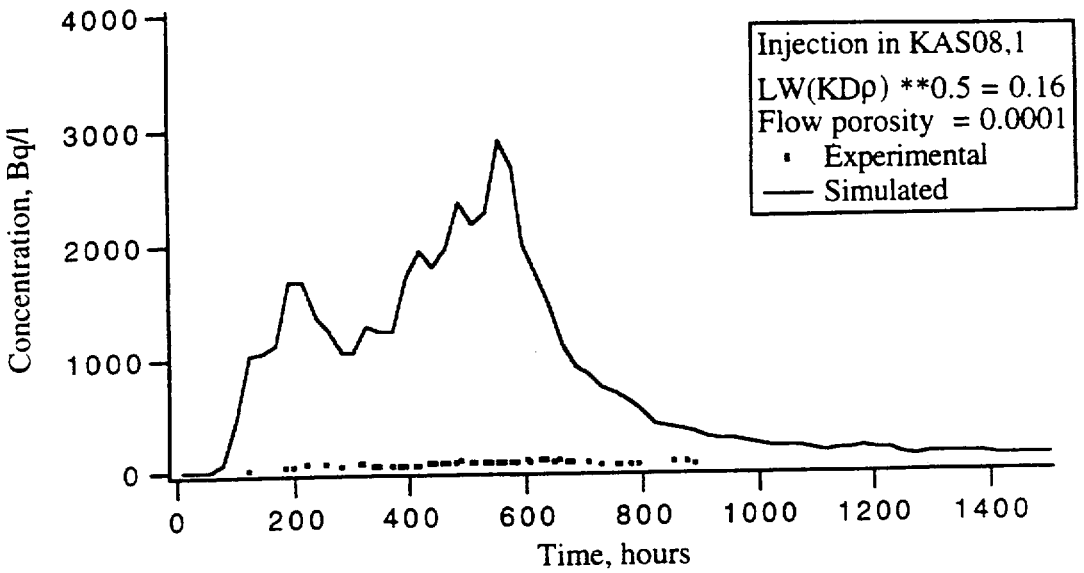

Figure 21. Simulated breakthrough curve of the tracer Rhenium injected in KAS08-1 for a flow porosity of 0.0001 and a value for G of 0.16.

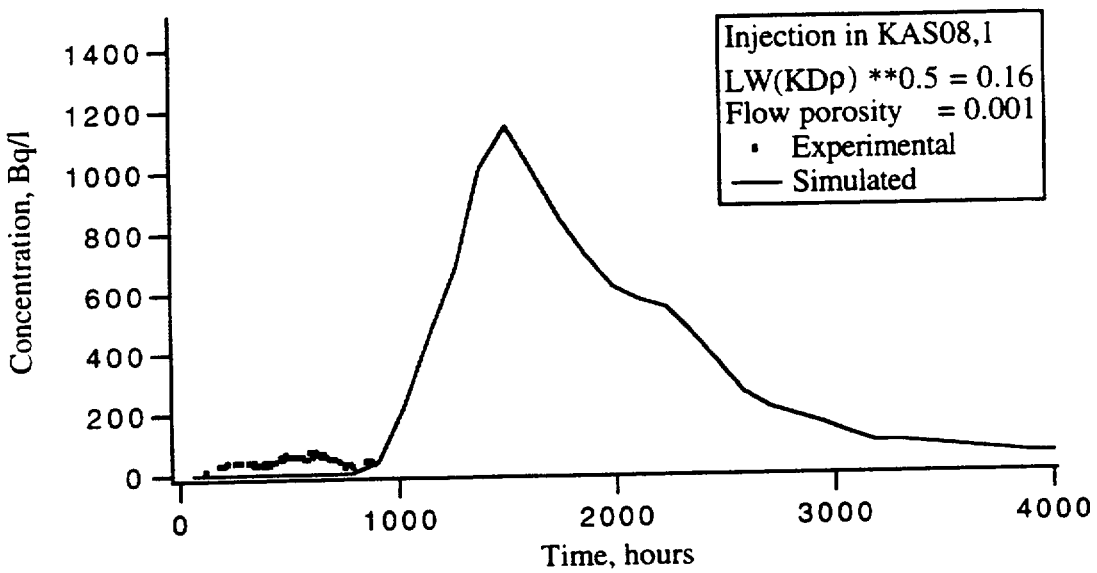

Figure 22. Simulated breakthrough curve of the tracer Rhenium injected in KAS08-1 for a flow porosity of 0.001 and a value for G of 0.16.

Simulated breakthrough curves for tracer tests which were not detected in the experiment.

Several injected tracers were not detected at the withdrawal hole. Simulations were, however, made for these tracer tests. In these simulations a flow porosity of 0.001 was

used. This value for the flow porosity was used because a smaller value (e.g. 0.0001) would mean a very short time for the early arrival. For the group G the value of 0.16 was used.

In these simulations, the local flow rates at the injection points were much higher than in the experiment (see Table 9). This means, in the experiment, that the tracers travel a certain distance with a very low flow rate and then the diffusion into the rock matrix play a much more important role.

The breakthrough curve for simulation of the Indium tracer injected in KAS02-4 is shown in Figure 23. The tracer was not detected in the field experiment in this test.

The breakthrough curve for simulation of Uranin tracer injected in KAS05-3 is shown in Figure 24. The tracer is believed to cause a second peak in the experimental breakthrough curve for Uranin (Rhén et al., 1992). The first peak in that plot is originated by the Uranin injected in KAS12-2.

The breakthrough curve for simulation of Iodine tracer injected in KAS07-4 is shown in Figure 25. The tracers arrive at the collection hole spread out in several peaks caused by the influence of the simulated intermittent decaying pulse injection. The tracer was not detected in the field experiment in this test.

The breakthrough curve from injection of Rhenium tracer in KAS08 section 3 did not result in any certain detection in the field experiment (Rhén et al., 1992). The simulated curve is shown in Figure 26.

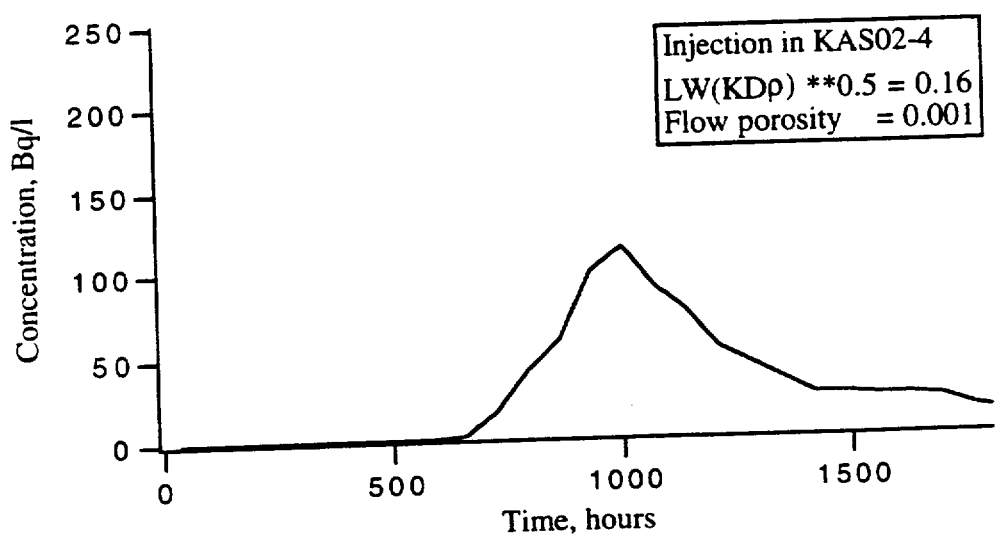

Figure 23. Simulated breakthrough curve for tracer Indium injected in KAS02-4. The tracer was not detected in the experiment.

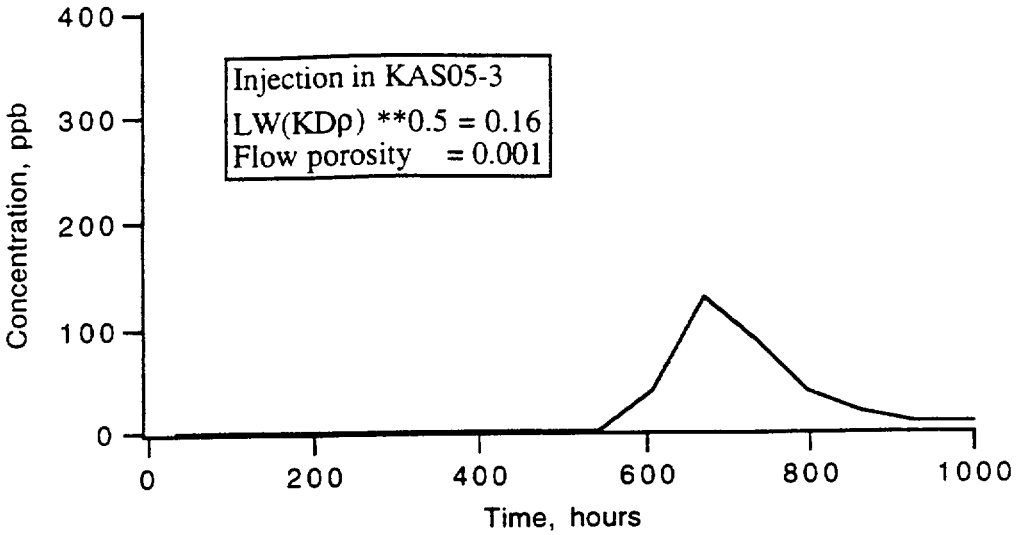

Figure 24. Simulated breakthrough curve for tracer Uranin injected in KAS05-3. The tracer was not detected in the experiment.

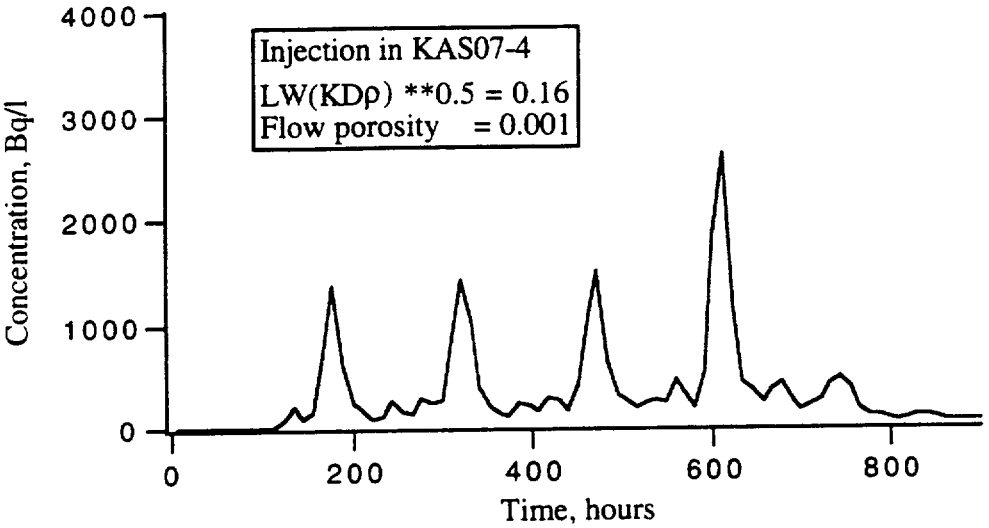

Figure 25. Simulated breakthrough curve for tracer Iodine injected in KAS07-4. The tracer was not detected in the experiment.

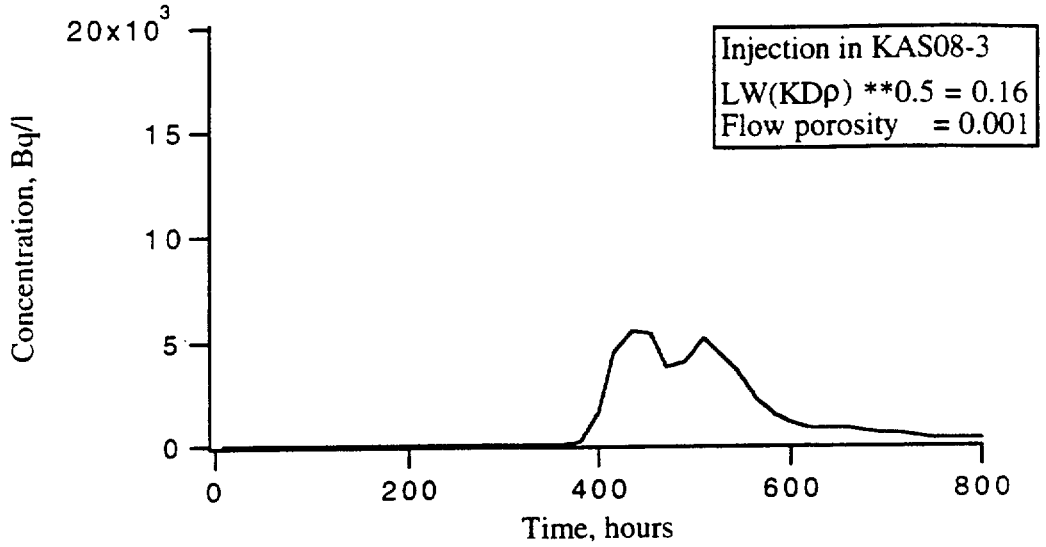

Figure 26. Simulated breakthrough curve for tracer Rhenium injected in KAS08-3. The tracer was not detected in the experiment.

7.2.3 Some possible reasons for the scant recovery in tracer tests

In most of the experimental tracer tests, the mass or activity of recovered tracer was very low. For example, for injection in KAS08, section 1 the recovery reached only 2-3 % of the injected activity, after correction by decay. In most of the other cases, no tracers were observed.

In this section, we discuss some different possible reasons for this low recovery. We will explore uneven flow distribution, matrix diffusion and flow porosity, and mention some other possible causes.

In our discussion, the breakthrough curve for Rhenium injected in KAS08-1 is used as an example. For this tracer test the breakthrough curve shows a clear peak at about 500 hours and two small peaks, one before and one after the main peak. The recovered tracer was only 2-3 % during the observation time.

Impact of uneven flow distribution

In a channel network with strongly varying conductances, the flow rate in the channels will also vary widely. The flow rate will span many orders of magnitude. This uneven flow distribution may cause a large dispersive effect. In this calculations, it is assumed that the water flow and solute transport occur only through those channels located in the fracture zones.

Moreno and Tsang (1994) found that when solutes are transported through a strongly heterogeneous porous medium with a very large standard deviation breakthrough curves showing multiple peaks could be found as in the channel network model. The first peak may come much earlier than the main mass of the the tracer.

The low recovery could be partially explained by an extremely uneven flow distribution, where the peak(s) observed in the experiment correspond(s) to a very early arrival of the tracer. The remainder of the injected tracer would arrive to the detection point after very long time. As the actual porosity distribution among the channels is not known, and the assumption we use, i.e. the cubic law, is dubious, uneven flow and porosity effects cannot be ruled out as a cause for the low recovery.

Impact of the diffusion into the matrix

When tracers are transported by the water flowing in the fractures, they may diffuse into the matrix. If the transport distances are large or the flow rates are small the impact of diffusion in the matrix is very large impact even for non-sorbing tracers. Tracers may also diffuse into pools of stagnant water in the fractures. This effect is similar to that caused by the diffusion into the matrix.

To explore and illustrate the impact of diffusion into the matrix, the solute transport in a single channel is used. Here the outlet concentration may be expressed as a function of the flow wetted surface, the effective diffusivity, and porosity of the matrix. For an injection during a short time interval (Δt), the solution for step injection may be used by subtracting two solutions delayed by Δt. If the rock properties are assumed to be constant, diffusion into the rock matrix is then a function of the flow wetted surface. The breakthrough curves were calculated for several values of flow wetted surface, from small to very large values.

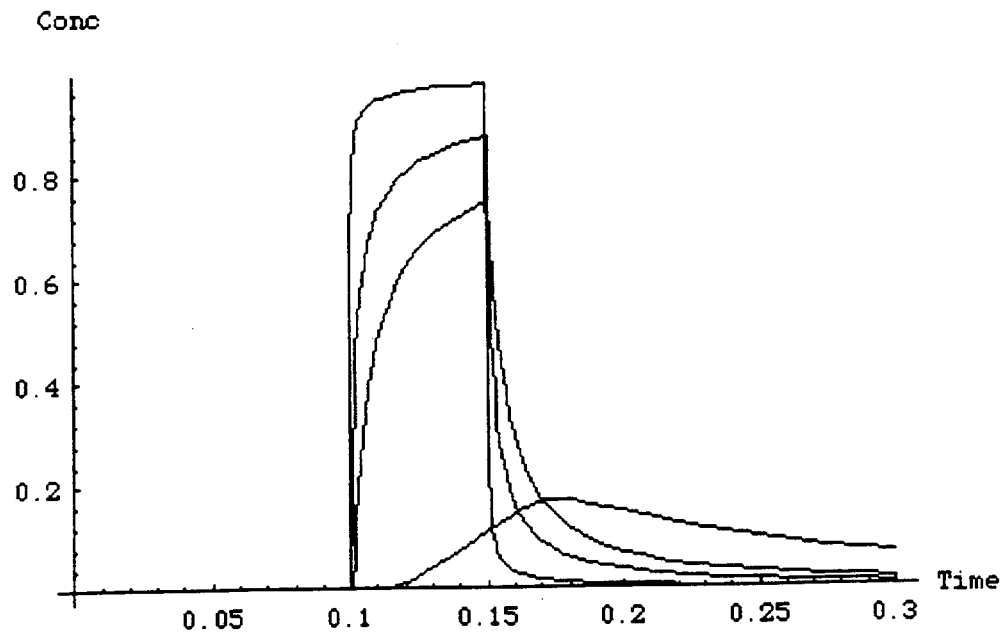

Figure 27. Simulated breakthrough curves for transport in a channel for values of the group G of 0.01, 0.05, 0.1, and 0.5. The flow in the channel was of 2.0 m^2/year and a injection time of 440 hours.

Figure 27 shows the breakthrough curves for an injection time of 0.05 years and a residence time of 0.1 years for several levels of diffusion into the rock matrix. The relationship between these times is rather similar to the relationship used in the experimental tracer test in KAS08-1. The breakthrough curves are wider when the diffusion into the matrix (flow wetted surface) is increased. A too large value for the flow wetted surface means that the curve is too wide, and does not agree with the shape of the experimental curve.

The tracer recovery in the simulated breakthrough curves was calculated for several values of the flow wetted surface. For the largest value possible to use to get an acceptable curve shape the recovery was about 50 - 60 % of the injected tracer. This means that diffusion into the rock matrix may only partly have caused the low recovery.

Impact of the flow porosity

For non-sorbing tracers that do not diffuse into the rock matrix, flow porosity is a critical parameter. It directly determines the mean residence time for the tracer. When the diffusion is strong the porosity is less important. So, for tracer tests with long travel distances and/or small flow rates in the channels the impact of the flow porosity may be negligible.

For flow through a channel network, the impact of flow porosity may be different depending of the flow wetted surface and flow rate in a specific channel or path. For

example, the part of the curve that corresponds to early arrival of the tracer is, in many situations, only little modified by an increase of the flow wetted surface. The reason for this is that the paths that transport the tracers with short arrival time have a large flow rate and only a small fraction of the tracer then diffuses into the rock matrix. On the other hand, flow porosity strongly influences the travel time through these paths.

Impact of the channel lengths

In order to test the influence of the channel length a single hypothetical fracture zone was simulated. The fracture carried a water flow and tracers were injected in one end and detected at the other end. Two values of the factor G was tested 0.16 and 1.6. The smaller value was used in the tracer simulations described above using the whole Äspö model. For each of the G-values the fracture zone was modeled with channel lengths of 5, 10 and 20 meters. For G = 0.16 the channel length had no clear impact at all. For G = 1.6 the channel length had some impact to the result. Using a shorter length resulted in a decrease of the concentration. The influence was, however, not dramatic.

8 DISCUSSION AND CONCLUSIONS

In general, the Channel Network Model can describe the water flow and solute transport in a fractured medium. In the model and in the field most of the flow and transport occur through the fracture zones. The transmissivity of the fracture zones is significantly larger than that of the rock mass.

In these simulations, the mean conductivities of the channels are obtained from data of Wikberg et al., (1991). The standard deviation is obtained from borehole data as shown in Chapter 6. This means that the drawdown data are not used to calibrate the model. Parameter variations are made to illustrate different effects.

The modelling is site specific in that sense that location and geometry of the fracture zones, fracture zone transmissivity, position of boreholes and boundary condition for the withdrawal borehole for the Äspö site are used. Borehole data from the Äspö Hard Rock Laboratory were used to determine the standard deviation in channel conductivity for channels within the fracture zones and to estimate the specific flow wetted surface. The mean hydraulic conductivity of the rock mass at Äspö is also used. The standard deviation in rock mass channel conductivity was assumed to be the same as for the fracture zone distribution. These two values for the rock mass have a small impact on the result since the fracture zones are responsible for most of the transport.

Simulations of drawdown.

The simulations of the pressure tests show that the boundary conditions in KAS06 may play an important role in the calculated drawdown. For example, if the experimental hydraulic head in KAS06 (-51.77 m) is used in the simulations a too high inflow to the withdrawal borehole is obtained. The simulated inflow is about 1.8 times the experimental inflow. For this situation the simulated drawdowns, in general, are larger than the experimental ones.

When the boundary condition, constant infiltration at the ground surface of the model, is used a high hydraulic head in the zones with low conductivity develops. Therefore, a larger transmissivity is used in the layer near the surface. This is supported by experimental data (KBS-3, 1983).

The simulated drawdown is, in most of the simulations, higher than the experimental values. This may be caused by a larger resistance around the borehole (e.g., skin effect).

Other reason may be erroneous boundary conditions. The best agreement was obtained when the determined inflow to KAS06 approach was used as a boundary condition in KAS06.

Simulations of tracer tests.

These simulations were performed with a given inflow to KAS06, a infiltration of 30 mm/year and a high conductive layer near the surface. As discussed above, no fitting or conditioning were done.
The simulated tracer tests with injection in KAS12, section 2, using a dye (Uranin) show a reasonably good agreement with the experimental data. Especially for the case with a flow porosity of 0.0001 and a value of the product $LW(K_d\rho_p D_e)^{0.5}$ equal to 0.16 a fairly good agreement is obtained, considering that no fitting at all has been done and that much of the data is estimated and not site specific. The concentration and recovery are, however, higher than the experimental ones.

When the tracer tests with injection of a radioactive tracer (Rhenium-186) in KAS08 section 1 is simulated, using the same parameter values as in the KAS12-2 simulation, the time for the first solutes to arrive is in some agreement with the corresponding experimental time. The simulated recovery is much higher than in the field test.

The recovery of the tracer in the experiment is very low, only a few percent of the injected activity. One explanation for the scant recovery of the tracer in the withdrawal hole could be that the observation time was too short, i.e. only the early arrival of the tracer was observed. Further mechanisms that may influence the recovery may be the impact of the uneven flow distribution, the diffusion in the rock matrix and the flow porosity. These processes are described more in detail in subsection 7.2.3.

Four of the experimental tracer tests gave no or no clear detection of tracer. All of these simulated tracer tests resulted in breakthrough curves. For the experiments with injections in KAS02-4 a fairly broad peak, with some tailing, came after about 1 000 hours. For the KAS07-4 tracer test simulation a pulse, very spread out in time, develops. The simulated test with injection in KAS05-3 resulted in a peak at a time of about 640 hours, though this tracer was not detected or weakly detected in the experimental breakthrough curve. We have no explanation for this result at present. A larger flow porosity and a larger diffusion into the rock matrix would give a breakthrough curve with smaller output.

For the tracer test with Rhenium injected in KAS08-3, which gave no observable detection in the withdrawal borehole, the simulated concentration is rather high (Figure 26) and

according to our simulation the tracer should have been detected in the experiment. One explanation could be that our model has better connection between KAS08-3 and the withdrawal hole KAS06 than corresponding in the field. One other reason for the small output of the tracers in KAS06, would be a too small value of the product $LW(K_d\rho_p D_e)^{0.5}$. For example, some small interaction of the rock with the tracer used (Rhenium-186) could explain the longer travel time and larger interaction with the rock matrix.

NOTATION

a_R	Specific flow wetted surface	m^2/m^3
C	Conductance	$m^4 \cdot s/kg$
D_e	Effective diffusion coefficient	m^2/s
K_d	Sorption coefficient	m^3/kg
L	Length	m
P	Pressure	$kg/(m \cdot s^2)$
Pe	Peclet number	
Q	Water flow rate	m^3/s
W	Channel width	m
r	Radial distance	m
t	Time	s
t_W	Water residence time	s
ε	Porosity	
μ_o	Mean logarithm of conductance	
ρ_p	Density of bulk rock	kg/m^3
σ_C	Standard deviation in the log-normal distribution of conductance	
σ_t	Standard deviation in the residence time distribution	s

REFERENCES

Birgersson L., Widén H., Ågren T., Neretnieks I., Moreno M. Site characterization and validation - tracer migration experiment in the validation drift. Report 2, part 1: Performed experiments, results and evaluation. Stripa Project Technical Report 92-03, SKB Jan 1992

Bäckblom G. (ed.), Almén K-E., Gustafson G., Rhén I., Stanfors R., Wikberg P. Äspö Hard Rock Laboratory, Status Report, Technical Document 25-93-013, 1993

Carslaw H.S. and Jaeger J.C. Conduction of Heat in Solids. Oxford University Press, Oxford, 2nd ed., 1959

Forsmark T. Information for numerical modelling 1992. General information and calibration cases for LPT2 and tests in KA1061A and KA1131B. SKB PR 25-92-14, 1992

Gylling B., Moreno L., Neretnieks I. Data requirements for the channel network model. SKB, Djupförvar, Projekt rapport PR 44-94-014. February 1994

KBS-3, 1983, Final storage of spent nuclear fuel, Report by Swedish Nuclear Fuel Supply Co, SKBF, Stockholm, Sweden, May, 1983

Levenspiel, O., Chemical Reaction Engineering, 2nd ed., pp 275. John Wiley, New York, 1972

Moreno L., Tsang Y.W., Tsang C.F., Hale F.V., Neretnieks I. Flow and tracer transport in a single fracture. A stochastic model and its relation to some field observations, Water Resour. Res., 24, pp 2033-3048, 1988

Moreno L., Neretnieks I. Fluid and solute transport in a network of channels, Journal of Contaminant Hydrology, 14, pp 163-192, 1993

Moreno L., Tsang C.F. Flow channeling in strongly heterogeneous porous media: A numerical study. Water Resour. Res., 1994 (In press)

Moridis, G. Personal communication. Lawrence Berkeley Laboratory, Berkeley, 1992

Neretnieks I. Diffusion in the Rock Matrix: An Important Factor in Radionuclide Retardation? J. Geophys. Res. 85, pp 4379-4397, 1980

Neretnieks I. A note on fracture flow mechanisms in the ground, Water Resour. Res., 19, pp. 364-370, 1983

Neretnieks I., Abelin H., Birgersson L. Some recent observations of channeling in fractured rocks. Its potential impact on radionuclide migration, In DOE/AECL conference Sept 15-17, 1987, San Francisco, Proceedings pp 387-410, 1987

Rhén I. (ed.), Svensson U. (ed), Andersson J-E., Andersson P., Eriksson C-O, Gustafsson E, Ittner T., Nordqvist R. Äspö Hard Rock Laboratory: Evaluation of the combined longterm pumping and tracer test (LPT2) in borehole KAS06, SKB Technical Report 92-32, 1992.

Robinson P.C., Connectivity, flow and and transport in network models of fractured media, Ph. D. Thesis, St. Catherine's College, Oxford University, Ref TP 1072, May 1984

SKB, Äspö Hard Rock Laboratory. Task Force on modelling of flow and transport of solutes. Data delivery no. 3 for Task no. 1, December 1992.

SKB, Äspö Hard Rock Laboratory. Task Force on modelling of flow and transport of solutes. Data delivery no. 4 for Task no. 1, February 1993.

Wikberg P. (ed.), Gustafson G., Rhén I., Stanfors R. Äspö Hard Rock Laboratory: Evaluation of the conceptual modelling based on the pre-investigations 1986-1990, SKB Technical Report 91-22, 1991.

Yamashita R., Kimura H., Particle-tracking technique for nuclide decay chain transport in fractured porous media, Journal of Nuclear Science and Technology, 27, pp 1041-1049, 1990.

APPENDIX A1

MODEL AND CODE SPECIFICATION

Name of the model:	Channel Network model. The code is written in Fortran 77.
Version:	Not applicable
Origin of the code:	The code is initially developed by Luis Moreno and Ivars Neretnieks, Department of Chemical Engineering and Technology, Royal Institute of Technology.

General description

The channel network is a 3D stochastic model based on the assumption that fluid flow and solute transport take place in a network of channels. In the model it is possible to include objects like fracture zones, borehole (and tunnels) in a simplified manner. The dispersion caused by differences in solute pathway properties, like channel flow velocity, is inherently built in to the model due to the stochastic generation of channel conductances. It is also possible to include solute and rock mass interaction processes, like sorption and diffusion into the rock matrix, in the simulations. The model is described more in detail in Chapter 3.

Conceptual and Mathematical model

Each member of the network is assigned a hydraulic conductance. This is the only entity needed to calculate the flow, if the pressure field is known. The conductance is defined as the ratio between the flow in a channel and the pressure difference between its ends. The pressure field is calculated by writing the mass balance at each channel intersection point. If the residence time for non-interacting solutes is to be calculated, then the volume of the channel members is needed as well. If sorption onto the fracture surface or diffusion into the matrix will be included in the model, the surface area of the flow wetted surface and rock properties must also be included.

Here, the conductances of the channel members are assumed to be log-normally distributed, with mean μ_0 and standard deviation σ_C. Different values are used for the mean conductance depending on where the channel members are located.

Numerical method

The large system of equations which are obtained are solved by a solver which uses the preconditioned gradient method (Moridis, personal communication, 1992). Some

standard routines such as RANDOM and SORT are also used. For the tracer test simulation a particle-following method is used (Moreno et al.,1988).

Limitations

The model is still at the development stage. The dispersion behavior of the model may be improved. The increasing dispersion length with distance which is seen in the field is not yet well described by this model or any other model except the Independent Channel model (Neretnieks, 1983).

Parameters required

- The distribution of conductances (the channel length is included in this entity).
- For non-interacting solutes the channel volumes or the flow porosity must be known.
- For the interacting solutes the flow wetted surface is an important entity.
- Properties of the rock are needed as well, such as rock matrix porosity, diffusivity, and sorption capacity for sorbing species (Neretnieks, 1980).
- Geometric information for objects like fracture zones and boreholes.
- Boundary conditions.

A more detailed description of the data requirements for the Channel Network model may be found in Gylling et al, (1994).

Type of results

The results can be obtained as pressure field, flow field (flow in each channel) and breakthrough curves for step or pulse injection. With small modifications the location of the tracer (particles) at a given time can be obtained.

Computer requirements

Any computer which may handle a Fortran 77 code and has a sufficiently large memory can be used. The memory requirement is quite large if the number of channels is large. For simulations of LPT2 we have used about 66 000 nodes or channel intersections. We have then used the memory required for storing about ten million real double precision variables and ten million integer variables.

User interface

For simulations of small rock volumes we have one program which is handling the pressure field, flow field and the particle following. For larger problems we have one

program for generating the pressure field which is then used for another program used for the tracer test simulations.

Code availability

The code is under development.

References:

- Moreno et al., 1988
- Moreno and Neretnieks, 1993
- Gylling et al., 1994

APPENDIX A2

Determination of flow wetted surface and channel length, for use in the the channel network model, using borehole data.

We assume that the rock contains a large number of randomly oriented channels. The channels have an average length, Z, and an average width, W. The channels are connected in some way forming a channel network through which the water flows. The fluid is in contact with both sides of the channel and the flow wetted surface for the average channel is then 2WZ. In a large rock volume with many channels an average specific flow wetted surface a_R m^2/m^3 can be defined. This is of interest for solutes which interact with the channel surfaces by sorption and/or matrix diffusion.

We first develop a method to determine the specific flow wetted surface by investigating how frequently an exploration borehole will hit a channel. We think in terms of having explored a borehole with some kind of test e.g. fluid injection in a narrowly spaced packer system. The testing procedure is such that in one packer interval there is essentially only one channel that is intersected. In practice a packer spacing of 1 m should be sufficient in the "good" rock although 3 m may also give fair information. In fracture zones a denser packer spacing might be warranted.

We do the analysis by determining in what volume of rock a randomly oriented average channel would intersect a borehole.

The rock contains a large number of channels which have an average length Z and an average width W as shown in Figure A1.

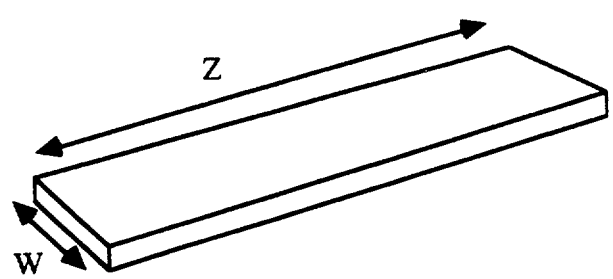

Figure A1. Definition of length Z and width W of a channel.

If there are a number of such channels in a volume of rock a borehole which is drilled in the rock may intersect some of them. We assume that the aperture of the channels is very small compared to the other dimensions of the channel and also that the widths of the channels are small in relation to the average distance between channels.

A channel may has any orientation in the space. A borehole will meet a such channel if it intersects the projected area of this channel on a plane perpendicular to the borehole

orientation. This projected area may be calculated it we known the average projection of the width and length of the channels.

The average width is obtained by integrating over all angles α. It is:

$$W_{av} = \frac{1}{\pi/2}\int_0^{\pi/2} W \operatorname{Cos} \alpha \, d\alpha = \frac{2}{\pi} W \tag{A1}$$

In the same way the average length in the other direction, Z_{av}, can be obtained at which a channel will intersect the hole.

The average length of the channel is obtained analogous to the width Equation (A1):

$$Z_{av} = \frac{1}{\pi/2}\int_0^{\pi/2} Z \operatorname{Cos} \beta \, d\beta = \frac{2}{\pi} Z \tag{A2}$$

The number of channels in a given rock volume has to be correlated to the frequency that channels are intersected by a borehole. To do this, the average projected area of the channels are distributed over a plane with a separation between them equal to the borehole diameter. This is shown in Figure A2.

Thus the average area, A_{av}, needed for that a channel will be intersected by a borehole is expressed below. This area includes the projection of the channel and the space occupied by the borehole itself:

$$A_{av} = Z_{av}W_{av} + (W_{av} + Z_{av})\, D_{bh} + D_{bh}^2 \tag{A3}$$

Using Equations A1 and A2 and neglecting the small area D_{bh}^2 the average area A_{av} may be approximated as:

$$A_{av} = \left(\frac{2}{\pi}\right)^2 ZW + \frac{2}{\pi} D_{bh} (W + Z) \tag{A4}$$

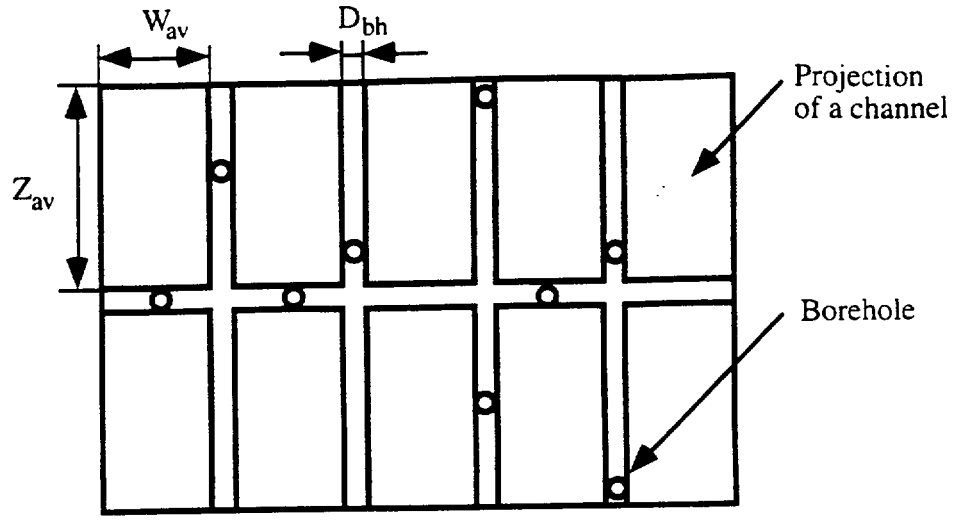

Figure A2. View of the projections of the channels, which may be found within the studied volume, on a plane perpendicular to the borehole.

If the average distance between channels intersected by the borehole has been obtained as H, then the average rock volume containing one channel is $H \cdot A_{av}$.

The specific flow wetted surface is the surface of the channel 2WZ in the rock volume $H \cdot A_{av}$. Thus:

$$a_R = \frac{2nWZ}{nA_{av}H} \tag{A5}$$

Here, n is the number of channels. Introducing the value of A_{av} from Equation A3, the following expression is obtained:

$$a_R = \frac{2WZ}{H\left[\left(\frac{2}{\pi}\right)^2 ZW + \frac{2}{\pi} D_{bh}(W+Z)\right]} \tag{A6}$$

The borehole diameter, D_{bh}, is a known entity and the average distance between the channels, H, that the borehole has intersected is known from the tests in the borehole.

If the channel width is known then a_R can be obtained. W is not, however, known unless independent observations have been made, e.g. in drifts and tunnels. Fortunately the specific flow wetted surface is not very sensitive to W provided $W \gg D_{bh}$ as can be seen from the Table A1. If $Z \gg D_{bh}$ Equation (A6) reduces to:

$$a_R = \frac{\pi^2}{2H} \tag{A7}$$

If the channel width is equal to the borehole diameter the specific surface would be overestimated by about a factor of 2.6 using Equation (A7).

Assume for a moment that the channel width is known and arrange the channels with length Z and width W in a cubic grid. In such a system of channels every cube with sides Z is delimited by 12 channels. Every channel is shared by four other cubes so there are three channels per volume of size Z^3. Thus:

$$Z^3 = 3\ H\ A_{av} = 3\ H\left[Z_{av}W_{av} + (W_{av} + Z_{av})\ D_{bh}\right] \tag{A8}$$

Inserting Equations (A1) and (A2) into (A4) gives:

$$Z^3 = 3\ H\ A_{av} = \frac{6}{\pi} H\left[\frac{2}{\pi} ZW + D_{bh}\,(W + Z)\right] \tag{A9}$$

If H, D_{bh} and W are known, then Z is obtained from Equation (A9). When Z>>W Equation (A9) can be simplified and Z may be obtained from:

$$Z^2 = \frac{6}{\pi} H\left[\frac{2}{\pi} W + D_{bh}\right] \tag{A10}$$

In summary: To assess the specific flow wetted surface of a rock borehole measurements are made with narrowly spaced packer tests. The spacing should be so narrow that essentially only one channel is intersected within the packed off section. What this means in practice will have to further be explored but at present it seems that a few meters should be sufficient. The average distance between channels H is then obtained. If the borehole diameter is small compared to the expected channel width then Equation (A7) gives the specific flow wetted surface. Otherwise the width W must be determined. When this is known the channel length is obtained from Equation (A9). Now all entities, W, Z, and D_{bh} needed in Equation (A4) are known and a_R is obtained from Equation (A6).

In the following example the procedure is illustrated.

Packer tests have shown that there is one channel intersection every 4 m, i.e. H=4 m. W is not known. Equation (A7) gives:

$$a_R = 1.23\ m^{-1}$$

Assume that D_{bh} = 0.08 m and W=0.2 m, what error would there be in a_R?

Equation (A9) gives

$$Z = 1.26 \text{ m}$$

A renewed determination of a_R using Equation (A6) gives

$$a_R = 0.76 \text{ m}^{-1}$$

Clearly the specific flow wetted surface would be somewhat overestimated if nothing is known about the channel width. At present the average channel width is thought to lie in the range of 0.02 - 0.5 m at most. What the resulting channel lengths and flow wetted surfaces would be using values in this range between these extremes are shown in Table A1. The result when W = Z is also included.

Table A1. Showing the influence of the channel width on the channel length and flow wetted surface.

W	Z	a_R
0.02	0.84	0.17
0.1	1.05	0.55
0.2	1.26	0.76
0.5	1.74	0.99
W=Z	4.86	1.23

It is seen from Table A1 that although the channel length will vary strongly if the width varies, the flow wetted surface is not very sensitive to variations in W.

List of International Cooperation Reports

ICR 93-01
Flowmeter measurement in borehole KAS 16
P Rouhiainen
June 1993
Supported by TVO, Finland

ICR 93-02
Development of ROCK-CAD model for Äspö Hard Rock Laboratory site
Pauli Saksa, Juha Lindh, Eero Heikkinen
Fintact KY, Helsinki, Finland
December 1993
Supported by TVO, Finland

ICR 93-03
Scoping calculations for the Matrix Diffusion Experiment
Lars Birgersson[1], Hans Widén[1], Thomas Ågren[1], Ivars Neretnieks[2], Luis Moreno[2]
1 Kemakta Konsult AB, Stockholm, Sweden
2 Royal Institute of Technology, Stockholm, Sweden
November 1993
Supported by SKB, Sweden

ICR 93-04
Scoping calculations for the Multiple Well Tracer Experiment - efficient design for identifying transport processes
Rune Nordqvist, Erik Gustafsson, Peter Andersson
Geosigma AB, Uppsala, Sweden
December 1993
Supported by SKB, Sweden

ICR 94-01
Scoping calculations for the Multiple Well Tracer Experiment using a variable aperture model
Luis Moreno, Ivars Neretnieks
Department of Chemical Engineering and Technology, Royal Institute of Technology, Stockholm, Sweden
January 1994
Supported by SKB, Sweden

ICR 94-02
Äspö Hard Rock Laboratory. Test plan for ZEDEX - Zone of Excavation Disturbance EXperiment. Release 1.0
February 1994
Supported by ANDRA, NIREX, SKB

ICR 94-03
The Multiple Well Tracer Experiment - Scoping calculations
Urban Svensson
Computer-Aided Fluid Engineering
March 1994
Supported by SKB, Sweden

ICR 94-04
Design constraints and process discrimination for the Detailed Scale Tracer Experiments at Äspö - Multiple Well Tracer Experiment and Matrix Diffusion Experiment
Jan-Olof Selroos[1], Anders Winberg[2], Vladimir Cvetkovic[2]
1 Water Resources Eng., KTH
2 Conterra AB
April 1994
Supported by SKB, Sweden